Upgrade of the readout electronics for the EDDA-Polarimeter at the storage ring COSY

Thesis
submitted in partial fulfilment of the requirements for the degree

Master of Science in Physics

Physics Institute III B

Faculty of Mathematics, Computer Science and Natural Sciences

RWTH Aachen University

Presented by

Fabian Hinder

Aachen, October 14, 2013

Thesis Supervisor:
Prof. Dr. rer. nat. Jörg Pretz

Abstract

This master thesis presents the development, installation and test of a new electronic readout system for the EDDA detector, used as an internal polarimeter in the COSY accelerator located at the Forschungszentrum Jülich. The implemented readout consists of a field programmable gate array (FPGA) placed on a VME board. The design of the developed firmware, running on the FPGA, is presented and tested. This firmware enables a polarisation measurement of the circulating particle beam in COSY by using elastic scattered protons or deuterons.

Data taken with the developed and installed readout electronics during two beamtimes in 2013 are presented. During the first beamtime in July, COSY was filled with an unpolarised proton beam. For the second beamtime in September, a polarised deuteron beam was available.

The first beamtime was used to test the programmed scalers by a comparison of the rates, measured with the existing electronics, and the ones, measured with the upgraded readout electronics.

In the September beamtime the upgraded readout electronics measured polarisation flips of a deuteron beam successfully. The spin flips of the deuterons were induced by a radio frequency solenoid.

The developed and installed system will be used by the JEDI collaboration to monitor the polarisation and spin evolution of particle beams, stored in COSY.

Contents

Nomenclature

CAEN	Costruzioni Apparecchiature Elettroniche Nucleari
CAMAC	Computer Automated Measurement And Control
CMS	Center of Mass System
COSY	COoler SYnchrotron
DAQ	Data Acquisition System
ECL	Emitter Coupled Logic
EDDA	Excitation function Data acquisition Designed for the Analysis of phase shifts
EDM	Electric Dipole Moment
FPGA	Field Programmable Gate Array
HRD	Half Ring Down
HRU	Half Ring Up
JEDI	Jülich Electric Dipole moment Investigations
LAB	Logic Array Blocks
LE	Logic Element
LUT	LookUp Table
LVDS	Low Voltage Differential Signal
NIM	Nuclear Instrumentation Module
PLU	Programmable Logic Unit
PMT	PhotoMultiplier Tube
RF	Radio Frequency
RMS	Root Mean Square
SCT	Spin Coherence Time
SM	Standard Model of particle physics
T-BMT	Thomas Bargmann Michel Telegdi
TDC	Time to Digital Converter
TTL	Transistor-Transistor Logic
VHDL	Very High speed integrated circuit Hardware Description Language

VME .... Versa Module Eurocard

1 Motivation & Introduction

Motivation

One of the unsolved problems in particle physics is the question: Why is our universe matter dominated?
The net baryon number divided by the number of photons, measured by the experiments COBE and WMAP, is [3]

$$\eta = \frac{n_B - n_{\bar{B}}}{n_\gamma} = 6.1^{+0.3}_{-0.2} \cdot 10^{-10}.$$

The Standard Model (SM) expectation for this ratio is of the order 10^{-18} which is eight magnitudes too low [17]. In 1967, Andrei Sakharov [19] formulated three conditions for baryogenesis:

1. Baryon number violating interactions early in the evolution of the universe,
2. non thermal equilibrium during the Baryon generation and
3. combined violation of the charge and parity ($\mathcal{CP}$) symmetry.

An electric dipole moment (EDM) of elementary particles, including hadrons, violate the parity ($\mathcal{P}$) and time reversal ($\mathcal{T}$) invariances. Assuming the $\mathcal{CPT}$ theorem a $\mathcal{T}$ violation is equal to a $\mathcal{CP}$ violation. The standard model predictions for EDMs of nucleons are of the order 10^{-31} to 10^{-32} e·cm, much below experimental sensitivities [17, 16, 10].

A measurement of a hadron EDM, not compatible with the SM prediction, could allow a deeper understanding of the matter dominated universe. A measurement is possible due to the effect, that an EDM $\vec{d}$ of charged particles in a storage ring leads to a tilt of the spin vector $\vec{S}^*$

$$\frac{\mathrm{d}\vec{S}^*}{\mathrm{d}t} = \vec{d} \times \vec{E}^*$$

by applying an electrical field $\vec{E}^*$ in the particle's rest frame [17].

The Jülich Electric Dipole moment Investigations (JEDI) collaboration, founded to measure EDMs of charged hadrons in storage rings, runs precursor experiments with polarised proton and deuteron beams in the COSY accelerator, located at Forschungszentrum Jülich.

Introduction

Accelerator experiments with polarised charged particles, like deuterons or protons, require an instrument to observe the polarisation during the acceleration and the storage of the particles. The polarisation monitoring system in the COSY accelerator at Forschungszentrum Jülich is the EDDA detector, built in the 1990s. The detector was designed to measure the elastic proton-proton scattering in an energy range of 0.5 GeV up to 2.5 GeV. Nowadays, the outer part of the detector is used as an internal polarimeter.

The detector, consisting of plastic scintillators, is readout by photomultiplier tubes whose signals feed electronic modules. These modules are readout by a data acquisition system. The core of the readout electronics consists of programmable logic units (PLUs) and scaler modules. Replacement equipment for these modules exist no longer. Therefore, a new system is intended to replace the programmable logic units and the scalers. This new system consists of a module with a field programmable gate array (FPGA) and a new scaler module.

The aim of this master thesis is the development of the firmware, running on the FPGA and the implementation of the FPGA module in the existing DAQ system.

This thesis deals with the following issues:

- The **Cooler Synchrotron** storage ring and the EDDA detector are detailed.
- The formalism to describe **Polarisation** of a particle beam is summarized and the way of measuring the polarisation is shown.
- The **Kinematics** of elastic scattered protons is explained and the resulting signature in the EDDA detector is derived.
- The chapter **Electronics** describes the electronic board holding the FPGA. Additionally, the programmed firmware being loaded in the FPGA is developed and explained.
- The results of a first function test of the programmed firmware are presented in the chapter **Functionality test of the firmware**.
- The measurement's results of unpolarised protons during the **Beamtime July 2013** are documented. A comparison of the old electronics and the new board verifies the correct working of the programmed FPGA.
- The chapter **Beamtime September 2013** presents polarisation measurements of a deuteron beam.

2 Cooler Synchrotron COSY

This chapter describes the accelerator, the COoler SYnchrotron (COSY), and the EDDA detector which is an internal detector in the storage ring.

2.1 Cooler Synchrotron storage ring

The COoler SYnchrotron COSY at Forschungszentrum Jülich is a storage ring with a circumference of 184 m applicable for protons and deuterons. COSY accelerates the particles to a momentum between 0.3 GeV/c and 3.7 GeV/c. An overview of COSY with the internal and external experiments is given in figure 2.1.

An ion source provides polarised protons or deuterons. These particles are accelerated in the cyclotron to a momentum of 300 MeV/c respectively 540 MeV/c. Following, they are transferred and injected to the storage ring being accelerated to the desired energy. The number of particles per fill is about 10^{10} for polarised and 10^{11} for unpolarised particles. Their polarisation can be measured before the injection by the low energy polarimeter. A measurement of the polarisation during the acceleration is possible with the internal EDDA detector. It is described in more detail in the next section.

An advantage of COSY is the beam phase space controlling. Therefore, COSY provides two methods of cooling the beam for different energy ranges. A beam with a momentum below 0.6 GeV/c can be cooled with the electron cooler. The stochastic cooler is used to manipulate the beam above a momentum of 1.5 GeV/c.

The width of the beam can be increased by heating it vertically or horizontally by applying a high frequency electric field perpendicular to the beam direction.

Besides the dipole magnets steering the beam in the arcs, COSY also provides magnetic quadrupoles to focus the beam and sextupole magnets to correct the beam position. A detailed description of COSY is given in [11] and [13].

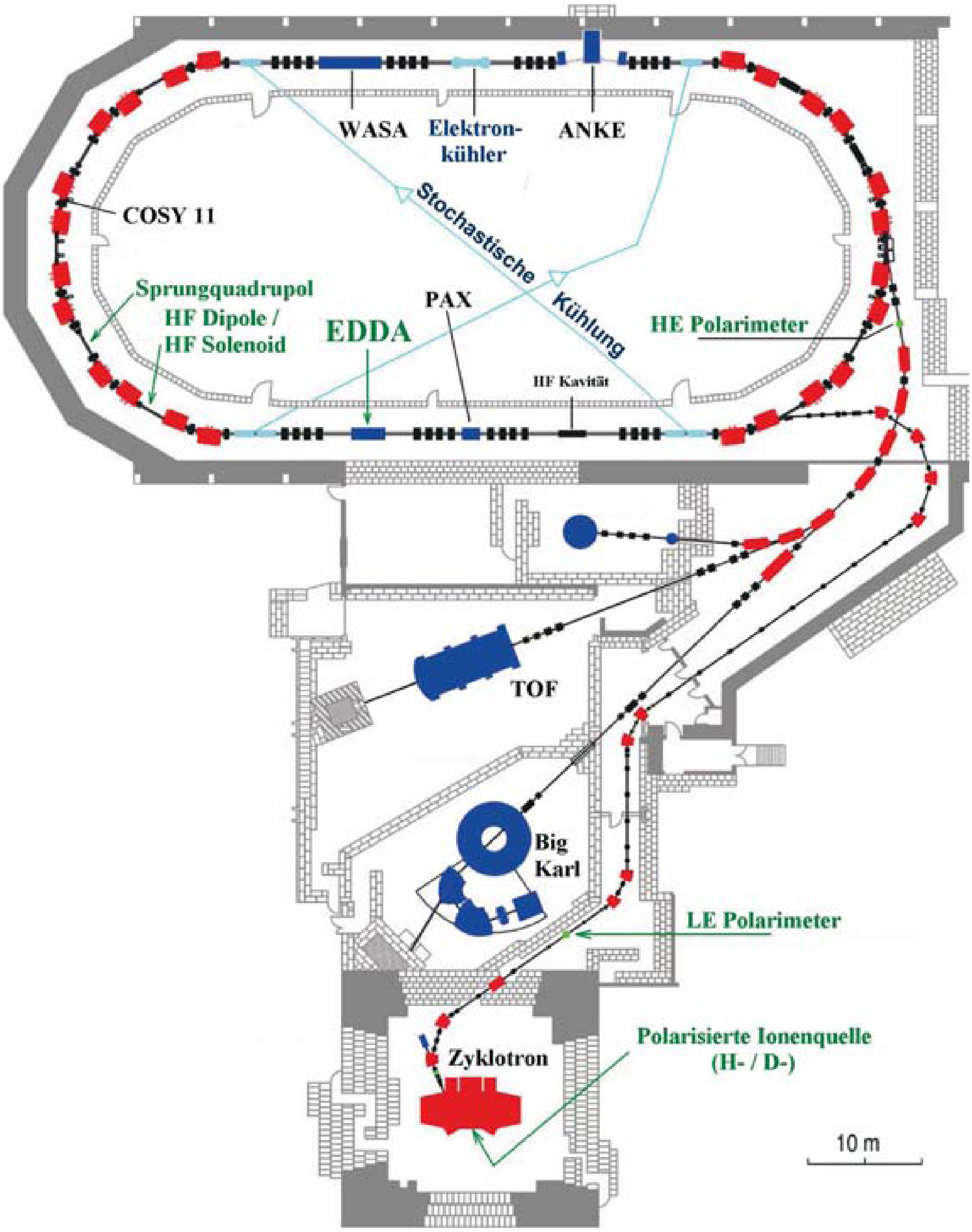

Figure 2.1: *COSY accelerator ring. [11, p. 56]*

2.2 EDDA detector

The EDDA[1] detector, was designed to measure the elastic proton-proton scattering, nowadays acts as an internal polarimeter at the COSY accelerator. The cylindrical detector surrounds the beamline with a radius of 160 mm and a length of 930 mm. The detector is built up of two layers. The inner one consists of 32 scintillating bars,

[1]Excitation function Data acquisition Designed for the Analysis of phase shifts

surrounded by 2 × 29 scintillating semirings. The bars enable an estimation of the difference in the azimuth angle ϕ of the scattered protons. The semirings measure the two scattering angles of the protons. A target, on which the scattering process takes place, can be installed downstream from the detector in the beam pipe. Figure 2.2 shows a schematic view of the detector.

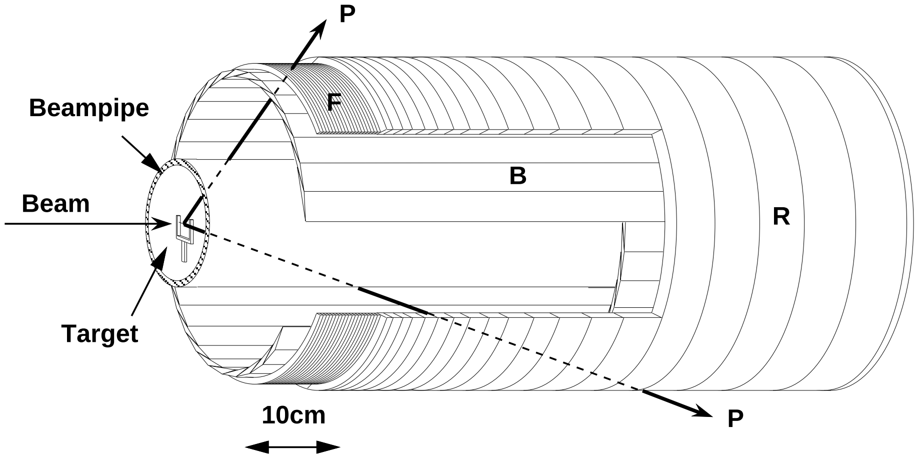

Figure 2.2: *EDDA detector with two elastic scattered protons. [8]*

2.2.1 EDDA coordinate system

Figure 2.3 shows the right-handed coordinate system used in the EDDA detector. The origin is set to the target position. The beam direction determines the z-axis. The x-direction points to the middle of the COSY ring and the y-direction points upwards. The scattering angle θ is measured in respect to the beam direction. The azimuth angle ϕ is measured clockwise starting at the x-axis. EDDA covers the full azimuth angle. The polar angle coverage is 9.9° to 72.4°.

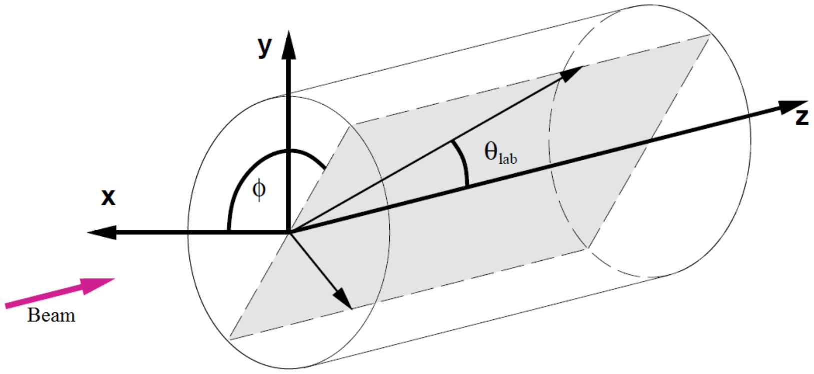

Figure 2.3: *Coordinates in the EDDA system. [22, p. 29]*

2.2.2 Readout of the scintillating detector elements

Each of the 32 bars, covering the azimuth angle range $\Delta\phi = 11.25°$, is readout upstream and downstream by photomultiplier tubes (PMTs). All of the bars are numbered in clockwise direction, starting with the one positioned at $\phi = 0°$.

The semiring numbering scheme starts at the ring closest to the target and pursues in beam direction. Each of the semirings 01 to 09 consists of a scintillating fibre double layer with a cross section of $2 \times 2\,\mathrm{mm}^2$. Four of the superimposed fibre pairs form one of the half rings. The other semirings 10 to 29 are constructed out of scintillating material. The half rings of the right side are readout by PMTs, connected via light guides to the bottom of the half rings ($\phi = 270°$, signal name HRD[2]). The half rings of the left side are connected to readout PMTs via light guides at the upper part of EDDA ($\phi = 90°$, signal name HRU[3]). Table 2.1 lists the angle ranges covered by all rings.

Table 2.1: *Angle ranges of the rings in the lab system. [21, p. 22] [12]*

Ringnumber	$\Delta\theta$	Ringnumber	$\Delta\theta$
01	72.4°..69.3°	02	69.8°..66.7°
03	67.3°..64.3°	04	64.8°..61.9°
05	62.5°..59.6°	06	60.3°..57.5°
07	58.1°..55.4°	08	56.1°..53.4°
09	54.1°..51.4°	10	54.9°..48.6°
11	52.1°..45.6°	12	49.3°..42.7°
13	46.4°..39.8°	14	42.7°..36.9°
15	39.8°..34.1°	16	36.9°..31.5°
17	34.1°..28.9°	18	31.5°..26.5°
19	28.9°..24.2°	20	26.5°..22.1°
21	24.2°..20.1°	22	22.1°..18.3°
23	20.1°..16.6°	24	18.3°..15.0°
25	16.6°..13.6°	26	15.0°..12.3°
27	13.6°..11.1°	28	12.3°..10.1°
29	11.1°..9.9°		

[2]HRD: Half Ring Down
[3]HRU: Half Ring Up

3 Polarisation

The following chapter summarizes the spin formalism of spin-$\frac{1}{2}$ and spin-1 particles. The method of measuring the polarisation of a proton beam by using calibrated effective analysing powers is additionally described.

3.1 Polarisation of a particle beam

3.1.1 Spin-$\frac{1}{2}$ particles

A spin-$\frac{1}{2}$ particle is represented by a normalized Pauli spinor with complex components a_1 and a_2 [14]

$$\chi = \begin{pmatrix} a_1 \\ a_2 \end{pmatrix}. \tag{3.1}$$

Whereas a particle, with a spin pointing in the direction of a chosen quantization axis (z), is described by a spinor with $a_1 = 1$ and $a_2 = 0$.

The expectation value of a hermitian operator Ω is defined as

$$\langle \Omega \rangle = \chi^\dagger \Omega \chi. \tag{3.2}$$

By defining the density matrix

$$\rho = \begin{pmatrix} |a_1|^2 & a_1 a_2^* \\ a_2 a_1^* & |a_2|^2 \end{pmatrix}, \tag{3.3}$$

the expectation value of Ω can be written as

$$\langle \Omega \rangle = \mathrm{Tr}\left(\rho \Omega\right). \tag{3.4}$$

The hermitian operators corresponding to a spin-$\frac{1}{2}$ particle are the usual Pauli operators [15]:

$$\sigma_1 = \begin{pmatrix} 0 & 1 \\ 1 & 0 \end{pmatrix} \quad \sigma_2 = \begin{pmatrix} 0 & -i \\ i & 0 \end{pmatrix} \quad \sigma_3 = \begin{pmatrix} 1 & 0 \\ 0 & -1 \end{pmatrix} \tag{3.5}$$

The expectation values of the spin matrices yield to a three component classical spin vector

$$\vec{S} = \frac{\hbar}{2} \begin{pmatrix} \langle \sigma_1 \rangle \\ \langle \sigma_2 \rangle \\ \langle \sigma_3 \rangle \end{pmatrix} . \tag{3.6}$$

For a beam comprising an ensemble of N particles a set of N Pauli spinors is defined by

$$\chi^{(n)} = \begin{pmatrix} a_1^{(n)} \\ a_2^{(n)} \end{pmatrix} \quad , n = 1 \ldots N. \tag{3.7}$$

The density matrix for the ensemble is

$$\rho = \frac{1}{N} \begin{pmatrix} \sum\limits_{n=1}^{N} \left| a_1^{(n)} \right|^2 & \sum\limits_{n=1}^{N} a_1^{(n)} a_2^{(n)*} \\ \sum\limits_{n=1}^{N} a_2^{(n)} a_1^{(n)*} & \sum\limits_{n=1}^{N} \left| a_2^{(n)} \right|^2 \end{pmatrix} . \tag{3.8}$$

Averaging the expectation values yields

$$\overline{\langle \Omega \rangle} = \frac{1}{N} \sum_{n=1}^{N} \chi^{\dagger(n)} \Omega \chi^{(n)} = \mathrm{Tr}\left(\rho \Omega\right) . \tag{3.9}$$

The density matrix can be expanded by using the Pauli matrices σ_i and the unity matrix I to

$$\rho = \frac{1}{2} \left(I + P_x \sigma_1 + P_y \sigma_2 + P_z \sigma_3 \right) . \tag{3.10}$$

The three coefficients P_x, P_y and P_z represent the spatial components in the chosen Cartesian coordinate system and are defined by

$$P_x = \langle \sigma_1 \rangle \tag{3.11}$$

$$P_y = \langle \sigma_2 \rangle \tag{3.12}$$

$$P_z = \langle \sigma_3 \rangle . \tag{3.13}$$

The vector $\vec{P} = (P_x, P_y, P_z)$ represents the polarisation of the beam. It is normalized and ± 1 are the limits for each component.

3.1.2 Spin-1 particles

Spin-1 particles have three possible eigenstates concerning a quantisation axis. Therefore, the spinor has to be extended to a three component spinor

$$\chi = \begin{pmatrix} a_1 \\ a_2 \\ a_3 \end{pmatrix} . \tag{3.14}$$

The corresponding spin operators are three 3×3 matrices [9, p. 18 -19]

$$S_x = \frac{1}{\sqrt{2}} \begin{pmatrix} 0 & 1 & 0 \\ 1 & 0 & 1 \\ 0 & 1 & 0 \end{pmatrix}, S_y = \frac{i}{\sqrt{2}} \begin{pmatrix} 0 & -1 & 0 \\ 1 & 0 & -1 \\ 0 & 1 & 0 \end{pmatrix}, S_z = \begin{pmatrix} 1 & 0 & 0 \\ 0 & 0 & 0 \\ 0 & 0 & -1 \end{pmatrix} . \tag{3.15}$$

Analogue to the expansion of the density matrix ρ for spin-$\frac{1}{2}$ particles, the expansion of ρ for spin-1 particles consists of nine hermitian 3×3 matrices. The three spin matrices and the 3×3 identity I are four of these matrices. The remaining five matrices can be constructed and written in a symmetric tensor of rank 2 by the following definition:

$$S_{ij} = \frac{3}{2} \left(S_i S_y + S_j S_i \right) - 2I\delta_{ij} \quad i, j \in x, y, z. \tag{3.16}$$

The expectation values of the operators S_i and S_{ij} yield to the polarisations

$$\begin{aligned} \text{vector polarisation: } P_i &= \langle S_i \rangle \\ \text{tensor polarisation: } P_{kl} &= \langle S_{kl} \rangle . \end{aligned} \tag{3.17}$$

The density matrix ρ in the expansion with these definitions is

$$\rho = \frac{1}{3} \left(I + \frac{3}{2} \sum_i P_i S_i + \frac{1}{3} \sum_{kl} P_{kl} S_{kl} \right) . \tag{3.18}$$

3.2 Polarisation measurement

For the description of the cross section in case of reactions with polarised beams, a definition of two coordinate systems is necessary. For an incoming particle with momentum $\vec{p}_{\text{in}}$ and an outgoing particle with momentum $\vec{p}_{\text{out}}$ the coordinate systems are shown in figure 3.1. The scattering coordinate system is stretched by the vectors $\vec{k}, \vec{s}$ and $\vec{n}$. The vectors $\vec{x}, \vec{y}$ and $\vec{z}$ form the EDDA coordinate system. The coloured plane is the scattering one, stretched by the momentum of the incoming particle $\vec{k}$

and the momentum of one outgoing particle $\vec{k}_1$. The described coordinates are defined by

$$\vec{k} = \frac{\vec{p}_{\text{in}}}{|\vec{p}_{\text{in}}|}, \quad \vec{n} = \frac{\vec{p}_{\text{in}} \times \vec{p}_{\text{out}}}{|\vec{p}_{\text{in}} \times \vec{p}_{\text{out}}|} \quad \text{and} \quad \vec{s} = \vec{n} \times \vec{k}. \tag{3.19}$$

The transformation between these coordinates and the EDDA-coordinate system is given by a rotation around the z axis by the angle ϕ. The polarisation of the beam described in the scattering system is given by [4, p. 17]

$$P_s = P_x \cdot \cos\phi + P_y \cdot \sin\phi \tag{3.20}$$

$$P_n = P_y \cdot \cos\phi - P_x \cdot \sin\phi \tag{3.21}$$

$$P_k = P_z. \tag{3.22}$$

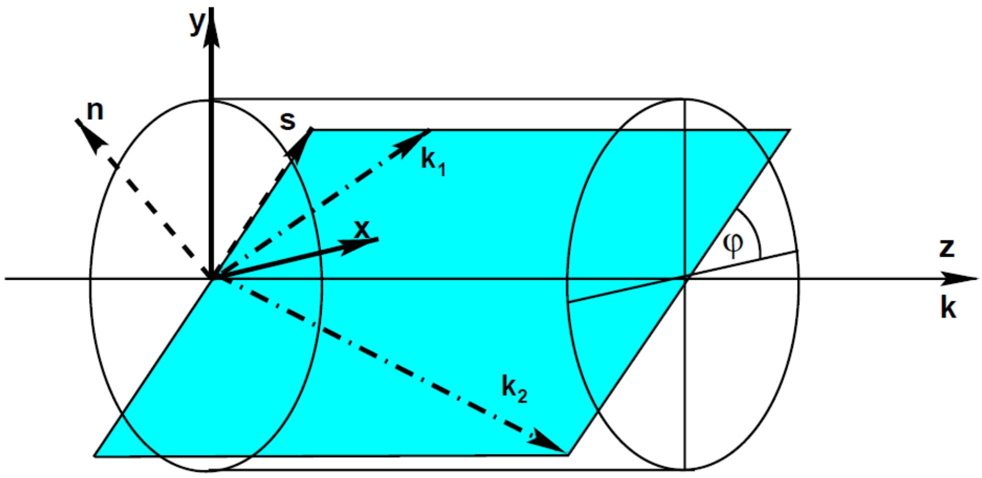

Figure 3.1: *Two scattered particles with momenta $\vec{k}_1$ and $\vec{k}_2$ in the EDDA detector. [4, p. 17]*

The cross section for the reaction of an unpolarised beam and an unpolarised target is independent of the azimuth angle ϕ. A polarised beam induces ϕ–dependence in the cross section, given by [9, p. 122]

$$\left(\frac{d\sigma}{d\Omega}\right)_{\text{pol.}} (\theta, \phi) = \left(\frac{\mathrm{d}\sigma}{\mathrm{d}\Omega}\right)_{\text{unpol.}} (\theta) \left(1 + \vec{A}(\theta) \cdot \vec{P}\right). \tag{3.23}$$

The polarisation of the beam is represented by the vector $\vec{P}$. The vector $\vec{A}$ describes the analysing power in the scattering coordinates. Due to the parity conservation in the electromagnetic and strong interactions the analysing powers A_s and A_z vanish [9, p. 138]. A polarisation P_y of the beam in y direction yields

$$\left(\frac{d\sigma}{d\Omega}\right)_{\text{pol.}} (\theta, \phi) = \left(\frac{\mathrm{d}\sigma}{\mathrm{d}\Omega}\right)_{\text{unpol.}} (\theta) \left(1 + A_y (\theta) P_y \cdot \cos \phi\right). \tag{3.24}$$

This cross section is maximal for scattering in the detector's left side ($\phi = 0°$) and minimal for scattering in its right side ($\phi = 180°$).

The counted events in the right and left (R, L) detector parts are proportional to the cross section integrated over the area covered by the detector elements Ω_{L} respectively Ω_{R}

$$L \propto \int\limits_{\Omega_{\mathrm{L}}} \left(\frac{\mathrm{d}\sigma}{\mathrm{d}\Omega}\right)_{\text{unpol.}} (\theta) \left(1 + A_y (\theta) P_y \cdot \cos \phi\right) \mathrm{d}\Omega \tag{3.25}$$

$$R \propto \int\limits_{\Omega_{\mathrm{R}}} \left(\frac{\mathrm{d}\sigma}{\mathrm{d}\Omega}\right)_{\text{unpol.}} (\theta) \left(1 + A_y (\theta) P_y \cdot \cos \phi\right) \mathrm{d}\Omega. \tag{3.26}$$

By means of the counted events, the polarisation of the COSY-beam can be determined for a known analysing power A_y by calculating the Left-Right asymmetry ϵ_{LR}

$$P_y = \frac{1}{A_y} \epsilon_{LR} = \frac{1}{A_y} \frac{L - R}{L + R}. \tag{3.27}$$

For a spin-1 particle beam, equation 3.23 is modified to

$$\left(\frac{d\sigma}{d\Omega}\right)_{\text{pol.}} (\theta, \phi) = \left(\frac{\mathrm{d}\sigma}{\mathrm{d}\Omega}\right)_{\text{unpol.}} (\theta) \left(1 + \frac{3}{2} \vec{A} (\theta) \vec{P} + \frac{1}{3} \sum_{kl} A_{kl} P_{kl}\right), \tag{3.28}$$

where A_{kl} is the tensor analysing power. With a purely vector polarised deuteron beam, as used in COSY, this equation simplifies to [9, p. 158]

$$\left(\frac{d\sigma}{d\Omega}\right)_{\text{pol.}} (\theta, \phi) = \left(\frac{\mathrm{d}\sigma}{\mathrm{d}\Omega}\right)_{\text{unpol.}} (\theta) \left(1 + \frac{3}{2} A_y (\theta) P_y \cdot \cos \phi\right). \tag{3.29}$$

The described formalism of measuring the polarisation for spin-$\frac{1}{2}$ particles is as well usable to measure spin-1 particles.

In addition to the measurement of the polarisation in y direction, a measurement of the horizontal polarisation (P_x) is possible by determining the Up-Down asymmetry. It is defined similarly to the Left-Right asymmetry with detector elements positioned at $\phi = 90°$ and $\phi = 270°$.

3.2.1 Effective analysing power

The analysing power depends on the scattering angle θ and the momentum of the beam p. For a fast measurement of the beam polarisation during the acceleration of a proton beam, effective analysing powers were determined by measuring the Left-Right asymmetry with a known beam polarisation for every ring [21]

$$A^{\text{eff}}\left(\Delta\theta^i_{\text{lab}}, p\right) = \frac{\epsilon\left(\Delta\theta^i_{\text{lab}}, p\right)}{P_y(p)}, \tag{3.30}$$

where $\Delta\theta^i_{\text{lab}}$ is the angle range covered by the ring i in the lab system. The known beam momentum and polarisation in y direction are p and P_y. These effective analysing powers allow a fast estimation of the beam polarisation for every ring by calculating the Left-Right asymmetry for every semiring pair i

$$P^i_y = \frac{1}{A^{\text{eff},i}} \frac{L^i - R^i}{L^i + R^i}. \tag{3.31}$$

The beam polarisation is given by the weighted mean of the polarisations, measured by every semiring pair. This combination is possible, since the polarisation of the beam is independent of the the detected protons' scattering angle.

4 Kinematics

The polarisation is measured by counting the elastic scattered protons in four different ranges of the azimuth angle ϕ. Therefore, an identification of the elastic scattered protons is necessary.

4.1 Elastic scattered protons

Figure 4.1 shows the signature of an elastic scattered proton event in the EDDA coordinate system. The elastic scattering of two particles with an identical mass is

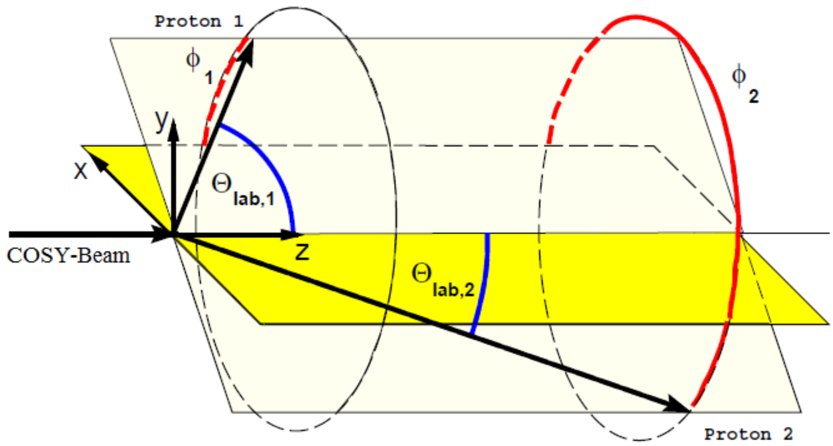

Figure 4.1: *Two elastic scattered protons in the EDDA coordinate system. [22, p. 16]*

completely described by two angles of a single outgoing particle, the scattering angle θ and the azimuth angle ϕ. The angles of the second particle are connected by the following equations[4]

$$\tan(\theta_1) \cdot \tan(\theta_2) = \frac{1}{\gamma_{\mathrm{CMS}}^2} \tag{4.1}$$

$$|\phi_1 - \phi_2| = \pi. \tag{4.2}$$

The factor γ_{CMS} is the Lorentz factor for a boost from the EDDA system into the center of mass system (CMS). These two conditions are used to identify the elastic scattered events and to trigger the scalers.

[4]A detailed derivation is given in appendix A.1

The relation of the two scattering angles depends on the momentum of the incoming proton. The dependence of the two angles is plotted in figure 4.2 for five different momenta of the incoming proton. Due to this energy dependence the trigger for the scalers has to change with the current momentum of the COSY beam.

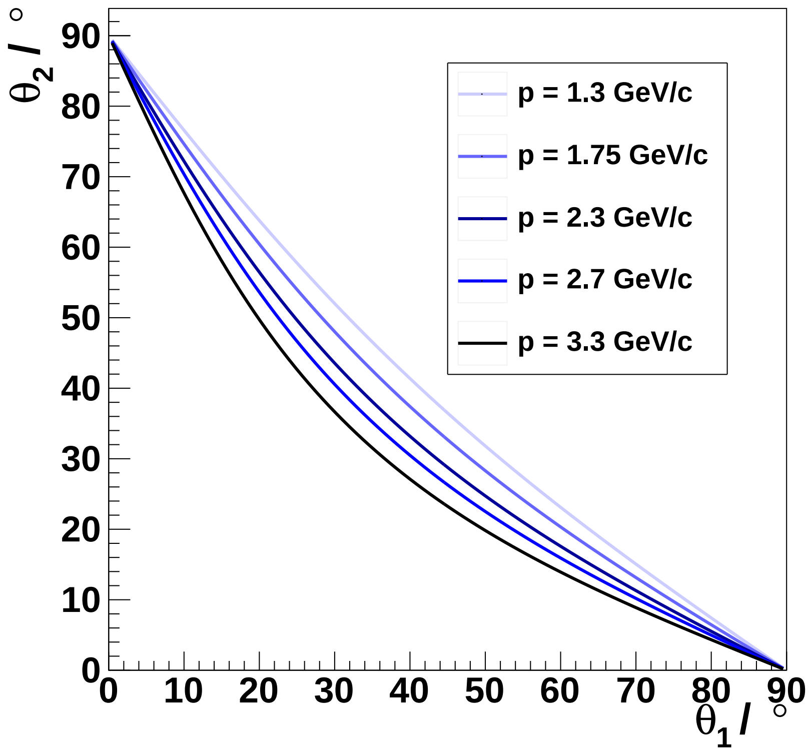

Figure 4.2: *Expectation of the scattering angles of two elastic scattered protons for different momenta.*

4.2 Signature of the elastic scattered protons in the semiring region of EDDA

The elastic scattered protons can be identified by the half rings of the EDDA detector. The left half rings cover a range of $-90° \leq \phi \leq 90°$, the right half rings cover the remaining 180°. Due to the coplanarity of the scattered protons, one proton is detected in the left half and the other one in the right half. The angles θ of both protons are measured by the semirings. Each semiring covers a range of the angle θ, therefore equation 4.1 yields combinations of kinematically allowed half rings. The filled areas in figure 4.3 correspond to the allowed combinations for four different momentum ranges of the COSY beam. The forward scattered proton is used to classify the detected event. If the proton is detected by one of the left semirings with

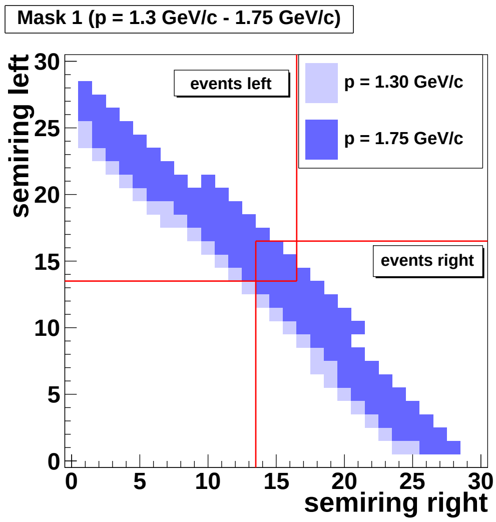

(a) $1.3\ GeV/c < p < 1.75\ GeV/c$.

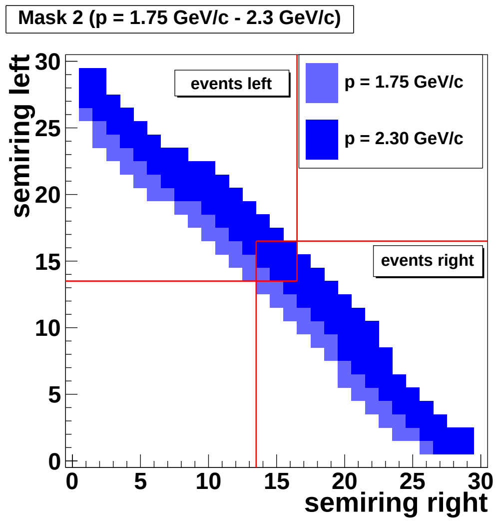

(b) $1.75\ GeV/c < p < 2.3\ GeV/c$.

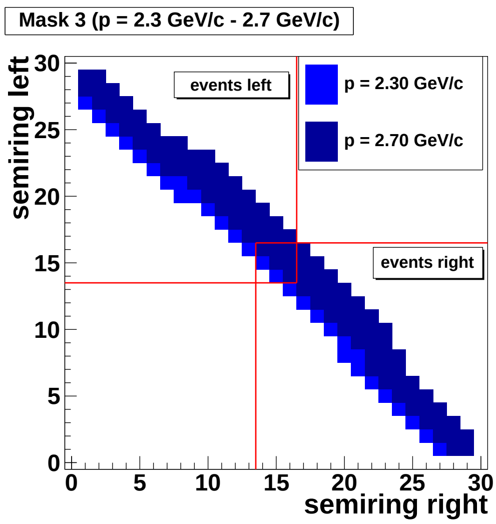

(c) $2.3\ GeV/c < p < 2.7\ GeV/c$.

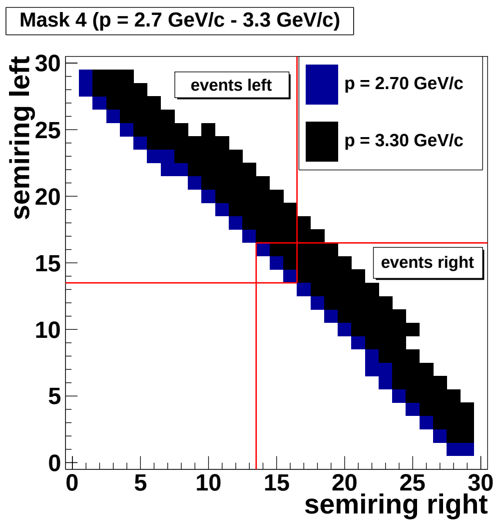

(d) $2.7\ GeV/c < p < 3.3\ GeV/c$.

Figure 4.3: *Signature of the events of elastic scattered protons in the EDDA detector for four different energy ranges.*

a number between 14 and 29, the event is categorised as a Left event. A proton in one of the right semirings with a number between 14 and 29 leads to a Right event. Therefore, all points lying in the red framed area are classified in the categories Left and Right. For a beam momentum below 1.3 GeV/c the events in the semirings 14 to 29 are directly counted without the condition of a kinematical coincidence. The five resulting momentum ranges are chosen because the effective analysing powers are known for these ranges.

The four shown patterns are used as masks in the electronics to select the elastic scattered events depending on the current beam momentum.

5 Electronics

This chapter describes the new readout electronic system, consisting of a VME[5] board holding an FPGA. First of all, the used VME board and its expansions are described. In the second section the functional principle of an FPGA is explained. The third part of the electronics chapter contains the development of the programmed firmware for the onboard FPGA.

5.1 V1495 general purpose VME board

The module V1495 produced by the manufacturer CAEN is a general purpose VME board. A photograph of the board is depicted in figure 5.1 (a). The board features four I/O sections (A, B, C and G) and three interfaces (D, E and F) to expand the module. The ports A and B are 32 bit wide LVDS/ECL/PECL[6] input channels. Port C is a 32 bit wide LVDS output. The two channels of port G can be used as input or output ports. These two channels accept logic signals in the TTL[7] or NIM[8] standard. Both the direction and logic level are selectable via the VME bus (cf. chapter 5.3).

On the interfaces D, E and F mezzanine boards can be mounted. In the configuration for the EDDA readout one A395A and two A395C boards are installed. The A395A board is a 32 bit wide LVDS/ECL/PECL input board. The A395C board provides a 32 bit wide ECL output. Detailed information about the V1495 module and the mounted boards can be found in manual [6].

The V1495 module is designed to perform different applications, handled by two FPGAs. One FPGA Bridge[9] controls the communication to the VME interface and the programming of the second FPGA User[10]. This User FPGA can be programmed with a custom firmware. All I/O sections and the three expandable interfaces are

[5]Versa Module Eurocard
[6]Standards for logic signals: LVDS: Low Voltage Differential Signal, ECL: Emitter Coupled Logic, PECL: Positive Emitter Coupled Logic
[7]TTL: Transistor-Transistor Logic
[8]NIM: Nuclear Instrumentation Module
[9]Altera Cyclone EP1C6Q2408N (Handbook: [1])
[10]Altera Cyclone EP1C20F400C6N (Handbook: [1])

directly connected to the User. Accordingly, this FPGA manages all input and output signals. Figure 5.1 (b) shows a schematic diagram of the FPGAs and the I/O sections.

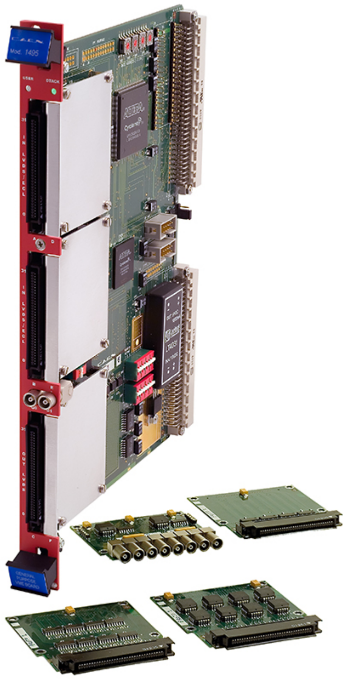

(a) *V1495 VME board and mezzanine cards. [7]*

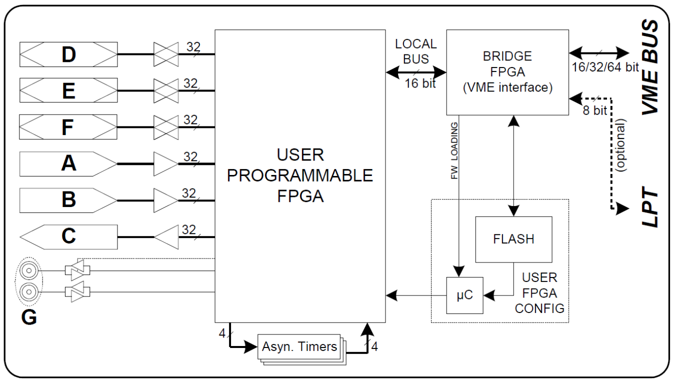

(b) *Block diagram of the V1495 module. [6, p. 7]*

Figure 5.1: *Photograph and a schematic view of the V1495 board.*

5.2 Field Programmable Gate Arrays

Field Programmable Gate Arrays (FPGA) consist of logic elements, configurable interconnections between these elements and memory blocks. All of these elements are programmable in the field by the user. In contrast to other programmable circuits, the number of reconfigurations of an FPGA is unlimited. Hence a direct test of the tailored firmware is possible. The smallest entity of an FPGA is a logic element (LE). One LE contains input signals, one lookup table (LUT), output signals and a 1 bit register (flip-flop) to hold the output signal. Figure 5.2 illustrates such a logic element.

The input signals are data signals and control signals. For example the register is controlled by the signals clock, reset and enable. The output signal is any operation on the four data channels. The LUT contains this operation. The output of the logical operation is directly linked to the output of the logic element or it is hold by the register. All logic elements of an FPGA are arranged on the chip in a two

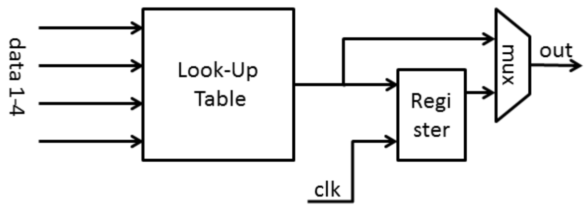

Figure 5.2: *Diagram of one logic element.*

dimensional array. In addition to these logic elements, an FPGA provides memory blocks to buffer signals. I/O ports of the FPGA realise the communication with other connected chips.

5.3 Programming the User FPGA

The I/O pins of the User FPGA are directly connected to the I/O ports of the V1495 board, so that all operations with these signals are implemented in the firmware of the FPGA. The entities which define the functions of the FPGA are written in the hardware description language, VHDL. The software package Quartus II[11] compiles the VHDL files and generates the firmware for the FPGA.

The program is split into small entities which fulfil special functions. These entities are also called components. All required components are instantiated by the main entity v1495_Logic and described in the following.

5.3.1 Entity v1495_Logic

The main entity v1495_Logic accesses all I/O ports of the board. The signals to select the direction and the type of logic levels for the ports D, E, F and G are also present. These signals are named SELD to SELG and nOED to nOEG. The 3 bit wide signals IDD, IDE and IDF identify the extension boards. The outputs nLEDG and nLEDR drive the two LEDs of the board (green and red). The local bus signals realises the communication to the VME FPGA. Table 5.1 summarizes all I/O signals of the entity v1495_Logic[12].

[11] Quartus II Version 10.1 Service Pack 1 Build 197 01/19/2011 SJ Web Edition
[12] The wiring of all used signals is summarised in tabular form in appendix A.2

Table 5.1: *Overview of all used ports of the Logic_V1495 entity.*

Port name	I/O	Width	Description
A	Input	32 bit	Signals from the I/O sections of the V1495 board
B	Input	32 bit	
C	Input	32 bit	
D	Input/Output	32 bit	
E	Input/Output	32 bit	
F	Input/Output	32 bit	
GIN	Input	2 bit	
GOUT	Output	2 bit	
nOED	Output	1 bit	Output enable of ports D, E, F & G 0: output 1: input
nOEE	Output	1 bit	
nOEF	Output	1 bit	
nOEG	Output	1 bit	
SELD	Output	1 bit	Level select of ports D, E, F & G 0: NIM 1: TTL
SELE	Output	1 bit	
SELF	Output	1 bit	
SELG	Output	1 bit	
IDD	Input	3 bit	Expansion id of ports D to F 000: A395A; 001: A395B 010: A395C; 011: A395D
IDE	Input	3 bit	
IDF	Input	3 bit	
nLEDG	Output	1 bit	Drivers for green/red LEDs 0: LED on, 1: LED off
nLEDR	Output	1 bit	

Different sub entities connect all mentioned signals to realise the main functions of the board:

v1495_Logic: Main entity, all I/O signals of the V1495 board are connected
coincRings: Entity processing the kinematical condition $\tan\theta_1 \cdot \tan\theta_2 = \frac{1}{\gamma^2_{\mathrm{CMS}}}$
coincRing_i: Entity identifying the kinematically allowed, opposite rings for ring i
coincRingBars: Entity combining the bar and ring signals
scalers: Entity implementing scalers
LB_INT: Entity for communication via the VME bus
memory: Memory module providing four masks for the coincRings entity

The coincidence of rings to determine the elastic scattering of the protons is realized in the coincRings component. One mask saved in the memory of the FPGA provides the information to determine the correct coincidence. Control signals select the mask for the current energy. The output of the coincRings module is split in two wires. One wire is connected to the output port F which is linked to the external VME scaler module. The other one feeds the input of the entity coincRingBars. This entity adds the information of the bars to the data stream.

The combined signal of bars and half rings is connected to the instantiated scalers component. This entity counts the detected coincidences for the each of the half rings HRU14 to HRU29 and HRD14 to HRD29 in four groups (Up, Right, Down and Left).

All control signals, scaler values, information about the board and the installed expansion cards are accessible via the instantiated local bus entity LB_INT. The local bus in and out signals are directly connected to the physical pins of the User FPGA which are wired to the Bridge FPGA. This scheme allows the communication between a control computer and the User FPGA via the VME bus. Figure 5.3 shows the connection scheme of the instantiated entities.

All signals out of the ring detector are coloured in red. The green arrows starting from port D are the incoming bar signals. The four arrows indicating the detected events in the Up, Right, Down and Left part of EDDA are coloured orange. Purple arrows illustrate the communication between the VME bus and the instantiated entities. All azure arrows depict control signals connected to port D. The direction of the arrows comply with the flow of the signals.

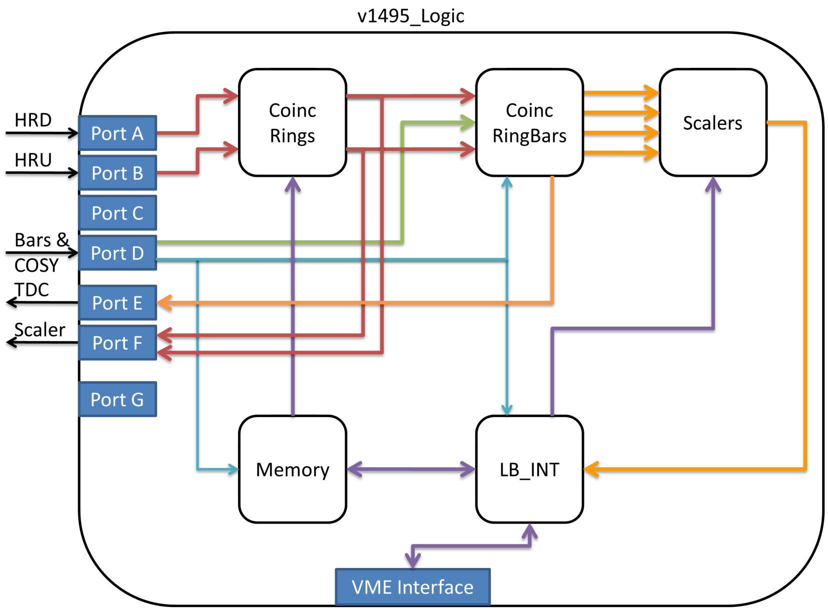

Figure 5.3: *Schematic drawing of the v1495_Logic entity.*

5.3.2 Processing the half ring signals

The coincRings entity implements the programmed kinematic condition. Listing 5.1 declares the coincRings input and output ports. The input ports, ringL and ringR, connect the half ring signals from the left and the right part of EDDA. The mask corresponding to the current energy is provided via the input port mask. The data type of the mask signal is an array with 29 29 bit wide vectors. This matrix is equal to the masks shown in chapter 4. The input bit directScalers changes between the direct loop through mode and the mask mode. The output ports are named leftTriggers and rightTriggers.

```
ENTITY coincRings IS
    PORT(
        ringL                : IN   std_logic_vector(28 DOWNTO 0);
        ringR                : IN   std_logic_vector(28 DOWNTO 0);
        mask                 : IN   MASK_RING_TYPE;
        directScalers        : IN   std_logic;
        leftTriggers         : OUT  std_logic_vector(15 DOWNTO 0);
        rightTriggers        : OUT  std_logic_vector(15 DOWNTO 0)
 );
END coincRings ;
```

Listing 5.1: *Port definitions of the coincRings entity.*

The architecture part of the entity (listing 5.2) implements the functions of this module. One of these functions is a multiplexer to change between the two operating

```
ARCHITECTURE RTL OF coincRings IS
    SIGNAL left    : std_logic_vector(15 DOWNTO 0); -- Temp signals for the
    SIGNAL right   : std_logic_vector(15 DOWNTO 0); -- left and right triggers

    BEGIN
        --direct loop through
        PROCESS(directScalers)
            BEGIN
                IF(directScalers = '1') THEN
                    leftTriggers   <= ringL(28 DOWNTO 13);
                    rightTriggers  <= ringR(28 DOWNTO 13);
                ELSE
                    leftTriggers   <= left;
                    rightTriggers  <= right;
                END IF;
        END PROCESS;

        genCoinc: FOR i IN 13 TO 28 GENERATE
            inst_coincRingLi: coincRing_i
                PORT MAP(ringL(i), ringR, mask(i), left(i-13));

            inst_coincRingRi: coincRing_i
                PORT MAP(ringR(i), ringL, mask(i), right(i-13));
        END GENERATE;

END ARCHITECTURE RTL;
```

Listing 5.2: *Architecture source code of the coincRings entity.*

modes: direct loop through and mask mode. The selector of the multiplexor is the directScalers bit. In case the directScalers bit is high, the outputs leftTriggers and rightTriggers are fed by the inputs ringL and ringR. This yields a counting of the events without a kinematical coincidence. The mode is used for a beam momentum below 1.3 GeV/c. In all of the other cases the outputs of the coincRing_i entities, described in the following, are linked to the outputs leftTriggers and rightTriggers.

The entity coincRing_i is built-up of OR– and AND–gates. Figure 5.4 is the corresponding block diagram. For each of the half rings the signals of the oppo-

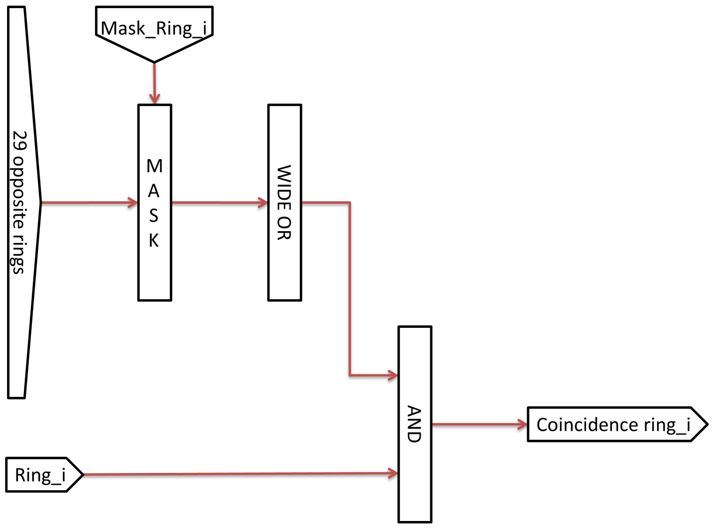

Figure 5.4: *Block diagram of the coincRing_i entity.*

site 29 detectors are masked with the corresponding mask. This is achieved by a bit–per–bit AND operation between the signals and the saved mask. A 29 bit wide OR gate reduces the width of the masked signal to one. If ring_i and the reduced signal are '1' at the same time, the output signal named coincidence ring_i is set to a high level.

Summarizing, these logical operations sift the kinematic coincidence between one half ring and the opposite 29 semirings. The kinematic coincidence is verified for the 2 x 16 half rings with the smallest angle respective the beam direction.

The resulting 32 channels are split up in two wires. One drives the output port F of the V1495 module which is connected to the external VME scaler module. This module allows a measurement of the Left-Right asymmetry without the bar signals. A combination of the gained 32 channels and all of the bars is necessary, to measure the Up-Down and Left-Right asymmetries with respect to the signals in the bars. The next section describes the implemented functions to merge these signals.

5.3.3 Combination of the bar signals and the masked half ring signals

The half rings of the detector distinguish only between events on the left and right side. Therefore, the 32 bars of the EDDA detector are needed to render a measurement of the polar angle ϕ possible. In general, a measurement of the polar angle with a resolution of around $360°/32 = 11.25°$ is possible. But for the EDM precursor experiment the signals from the bars are combined in eight packages of four bars leading to a resolution of only 45°. This combination is done for the front and back readout of the bars. The resulting 2×8 signals are connected to port D of the V1495 board.

Internally, these signals are connected to the entity coincRingBars. The main function of the entity is to sort the events in the four category groups Up, Right, Down and Left. These categories involve the ϕ angles in the EDDA coordinate system: $-45°$ to $45°$, $45°$ to $135°$, $135°$ to $225°$ and $225°$ to $315°$. For this purpose, the wires out of the bars are sorted in six categories (Up-Right, Right, Down-Right, Down-Left, Left and Up-Left). This is done in two different modes: one mode for a single detected particle and one mode for two detected particles. The six bar categories are then combined with the rings to form the mentioned four classes.

The flow of the signals through the logic functions of this entity is shown in the figures 5.5 to 5.7. Additional inputs of the entity are two control bits (directScalers and enableEDMTrig), the signals out of the coincidence of the rings (ringLTrig and ringRTrig) and four trigger bits from the EDM wiring of EDDA (edmTriggers). The functions of all of these inputs are explained in the following paragraphs.

Combination of front and back readout: First of all the 2×8 signals of the front and back readout of the bars, labelled barF and barB, are reduced to eight signals by an OR operation. In the following these resulting eight signals are referred to as bar 0 to bar 7. Figure 5.5 is the corresponding circuit diagram.

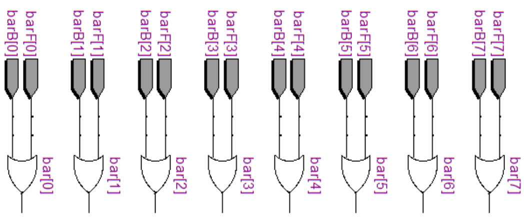

Figure 5.5: *Logical OR between the signals out of the front and back readout of the bars.*

Operating mode below 1.3 GeV/c: This mode is used for beam particles with a momentum below 1.3 GeV/c. A high directScalers bit selects this operating mode. The wiring, shown in figure 5.6, sorts the signals in the six mentioned categories. The Up-Right category corresponds to a signal in bar 0; the Right class is a signal in bar 1 or bar 2. Bar 3 is connected to the Down-Right category. The bars 4 to 7 are connected in a similar way to the three categories Down-Left, Left and Up-Left.

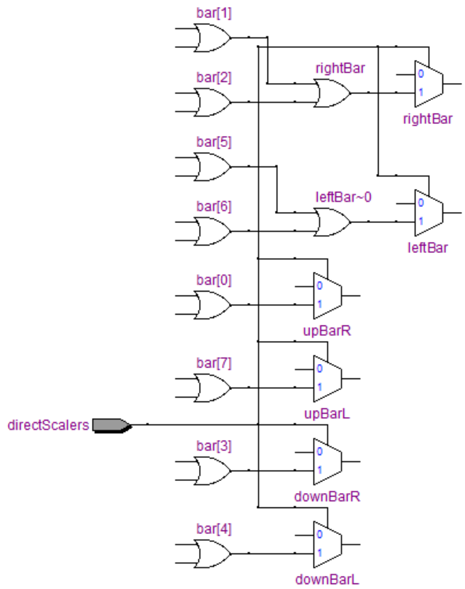

Figure 5.6: *Circuit of the bars to sort the incoming pulses in the six categories (Up-Right, Right, Down-Right, Down-Left, Left and Up-Left) for a high directScalers bit.*

Operating mode above 1.3 GeV/c: If the directScalers bit is low, signals out of opposed bars have to fulfil a coincidence condition. The wiring for this case is shown in figure 5.7. A logical AND operation between opposite bars achieves this condition. The category Up-Right corresponds to a signal in bar 0 and bar 4. The Left category is a combination of bar 2 and bar 6 or bar 1 and bar 5. A signal in the bars 3 and 7 defines the Down-Right class.

Only the information of the bars cannot distinguish between the two detected particles. For this reason, the categories Up-Right, Down-Left; Left, Right and Down-Right, Up-Left are pairwise equal. For a correct mapping the information of the rings is needed.

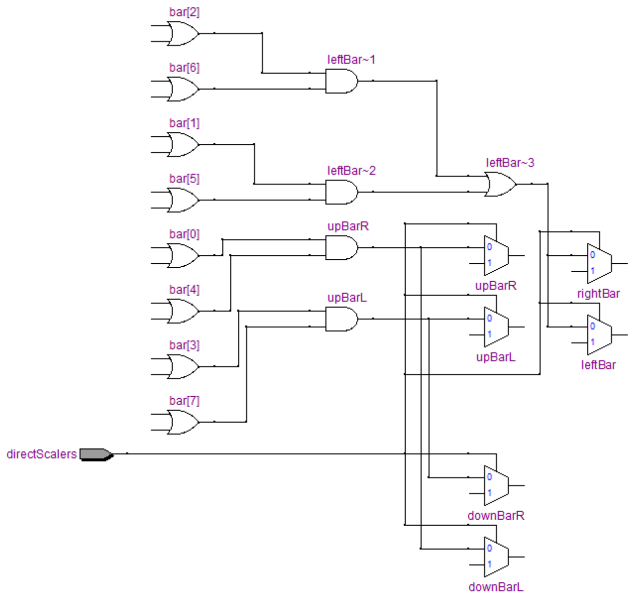

Figure 5.7: *Wiring to sort the incoming signals in the six categories (Up-Right, Right, Down-Right, Down-Left, Left and Up-Left) with respect to a detection of both particles in the bars.*

Combination of the bars and the half rings: To every hit in the bars corresponds a hit in one half ring. The information of both systems allows a determination of the two angles ϕ and θ of the scattered particle. The angle θ correlates to the number of the active half ring. The angle ϕ is decoded in the four ranges Up, Right, Down and Left. The events for the lowest 16 semirings are recorded by counting the rates in the four ϕ sections. The signals to be counted are a combination of the bar signals and the half ring signals. Figure 5.8 shows exemplarily the wiring for the four sectors for the semirings left 14 and right 14.

The category Up is active for a hit in the right semiring and in the Up-Right bar sector or for a hit in the left semiring and a hit in the Up-Left bar sector (figure 5.8 (a)).

The Down signal is a similar combination of the semirings and the Down bar sectors (figure 5.8 (c)).

The Right and Left signals are a coincidence of the Right bar sector and the right semiring respectively a coincidence of the Left sector and the left semiring (figures 5.8 (b), (d)).

Four additional signals, the EDM triggers for each of the sectors, are included for a high enableEDMTrig bit. These four signals are outgoing signals of the electronics used for the precursor EDM experiment [20]. These electronics identify detected

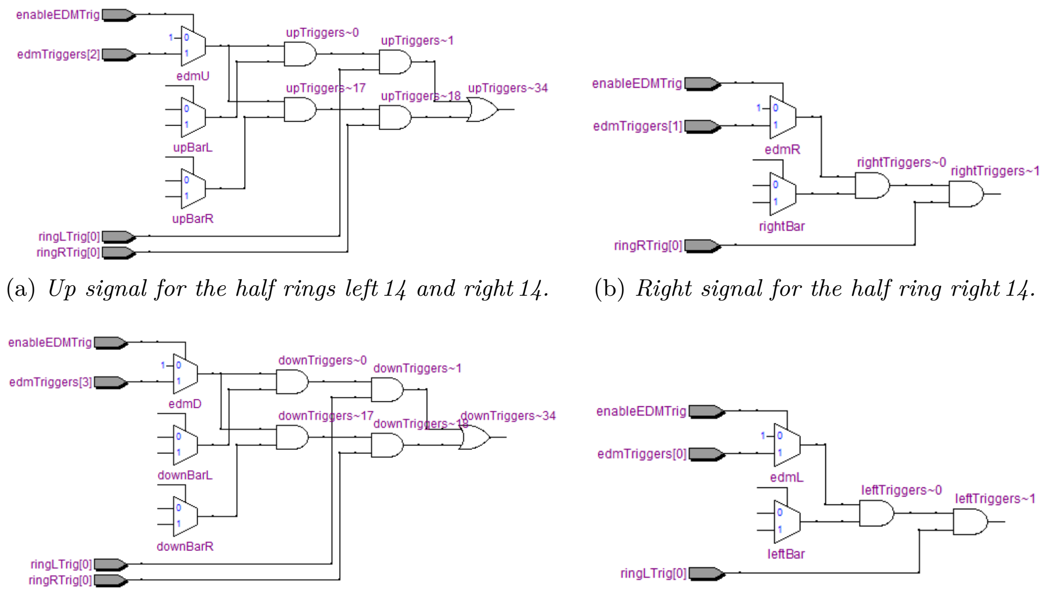

(a) *Up signal for the half rings left 14 and right 14.* (b) *Right signal for the half ring right 14.*

(c) *Down signal for the half rings left 14 and right 14.* (d) *Left signal for the half ring left 14.*

Figure 5.8: *Circuits to combine the signals of the bars and the two semirings (left 14 and right 14). A high enableEDMTrig bit takes account of the edmTriggers.*

deuterons in the four ϕ categories by measuring the energy deposition in the bars and the four most forward rings.

The signals for the other 2×15 semirings $(15-29)$ are produced in a similar way. All in all, this leads to 16 signals for each of the sectors Up, Right, Left and Down. All of the 16 signals of each sector are grouped in one vector connected to the output of the entity coincRingBars.

These 4 16-bit wide vectors are the channels to be counted by the implemented scalers and readout by the data acquisition system.

5.3.4 Scalers

To determine an asymmetry in the detected rates the outgoing signals of the entity coincRingBars are connected to the scalers entity. The implemented scalers instantiate all required functions to count the 4×16 signals and to readout the current values.

The port definition of the scalers entity is shown in listing 5.3. The input ports of the scalers entity are the leftTriggers, rightTriggers, downTriggers and upTriggers ports which are fed by the 4×16 outgoing channels of the previously described entity. The ports readout and reset control the behaviour of the scalers. The output buses leftScalers, rightScalers, upScalers and downScalers hold the counted events per channel.

```
ENTITY scalers IS
    PORT(
        leftTriggers  : IN   std_logic_vector(15 DOWNTO 00);
        rightTriggers : IN   std_logic_vector(15 DOWNTO 00);
        upTriggers    : IN   std_logic_vector(15 DOWNTO 00);
        downTriggers  : IN   std_logic_vector(15 DOWNTO 00);
        readout       : IN   std_logic;
        reset         : IN   std_logic;
        leftScalers   : OUT  SCALERS_TYPE;
        rightScalers  : OUT  SCALERS_TYPE;
        upScalers     : OUT  SCALERS_TYPE;
        downScalers   : OUT  SCALERS_TYPE
    );
END ENTITY;
```

Listing 5.3: *Port definitions of the scalers entity.*

For each of the signals in the four incoming vectors one scaler is generated. Figure 5.9 illustrates the generated scaler for the left semiring 15.

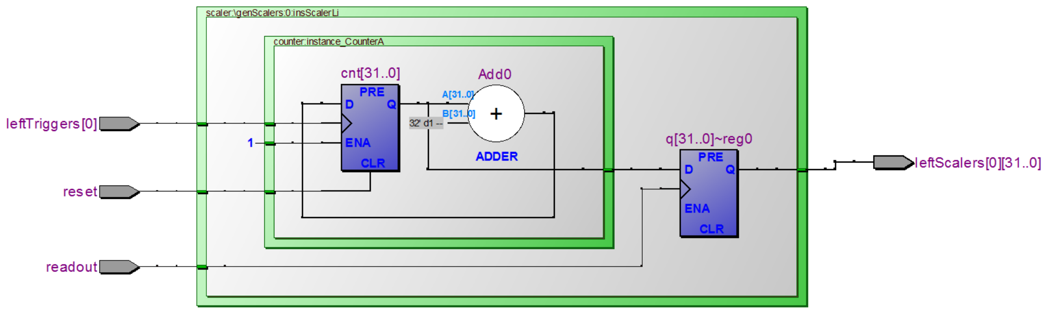

Figure 5.9: *Circuit of the scaler module for channel Left 0 (semiring left 14).*

Each signal of the four vectors drives the clock port of the corresponding scaler. The reset ports and the readout ports of all scalers are connected to the incoming reset and readout ports. Every instantiated scaler has one output port connected to the corresponding element of one of the four outgoing vectors.

Each scaler module counts the number of rising edges on its clk port and saves the value internally in a 32 bit wide register. A rising edge on the port readout shifts the internal value of the register to port q which is connected to the corresponding output of the scalers module. Since all scalers are driven by the same readout signal, a high readout saves the values of all scalers at the same time. These values are accessible via the VME bus interface.

During the readout the counter works without restrictions. Thus all detected events are counted dead time free. All scalers are reset by a high reset bit which is fed by the global reset signal of the scalers entity.

5.3.5 Local bus interface

The local bus interface provides the communication between the User FPGA, its entities and the VME bus. This local bus entity adapts to the example entity of the delivered gate pattern firmware [5]. All data communication is organised in writing and reading accesses to specific registers. All used register addresses are listed in table 5.2. The shown registers and their functions are described in detail in the following paragraphs.

Table 5.2: *Map of all used registers and addresses.*

Address	Read/Write	Name	Content
`0x1000`	R	REG_INFO	V1495 board status
`0x1004`	R/W	Reg_MASKPortE	mask output port E
`0x1008`	R/W	REG_CTRL	control all entities
`0x1010`	R/W	REG_READOUTCOUNTERS	control the counters
`0x1048` – `0x1084`	R	scalerL13 - scalerL28	left scaler values
`0x10BC` – `0x10F8`	R	scalerR13 - scalerR28	right scaler values
`0x1100` – `0x1170`	R/W	MASK0 - MASK28	write and read masks for all rings
`0x1180` – `0x11BC`	R	scalerU13 - scalerU28	up scaler values
`0x11C0` – `0x11FC`	R	scalerD13 - scalerD28	down scaler values

Info register: The info register contains information on the installed mezzanine boards, the loaded User FPGA firmware and the currently selected mask for the half rings coded in the lower 16 bit of the register. The used coding scheme is listed in Table 5.3.

Mask the output port E: The first four channels of port E which is cabled to an external Time to Digital Converter (TDC) are driven by the four vectors Up, Right, Down and Left coming out of the entity coincRingBars. The aim of this cabling is to generate time stamps for all events of the four categories. The outgoing vectors of the coinRingBars entity are all 16 bit wide where each bit corresponds to a certain

Table 5.3: *Coding of the info register.*

Bit	Content
15–13	selected mask for the rings
12–09	firmware version
08–06	IDD of expansion board in slot F
05–03	IDD of expansion board in slot E
02–00	IDD of expansion board in slot D

range in θ. The signals feeding the TDC should correspond to the θ ranges with the highest analysing power and statistics. To select these θ ranges out of the four categories a bit-per-bit AND operation between each of the four 16 bit wide vectors and the mask buffered in REG_MASKPortE is proceeded. A wide OR operation between these resulting 16 channels per category drives the corresponding channel of port E.

For instance, an OR operation between the first four elements of each vector is selected by the mask with the content `0x000F`. In this configuration, a detected signal in one of the lowest four rings of the four categories sets the corresponding port E to a high level. This detected event is then marked with a time stamp in the TDC and saved with the DAQ.

Control register: The lowest 14 bits of the control register control several functions of the whole device. Table 5.4 documents the mapping of this register.

Table 5.4: *Control register map.*

Bit	Signal name	Function
13	enableEDMTrig	enable the edm trigger
12	enableLoadMasks	enable load mask from memory
11	RamWren	enable writing masks to memory
10–08	RamAddress	address of mask for write/read from memory
07	nOEG	enable output of port G (0:Output, 1:Input)
06	SELG	select port level G (0:NIM, 1:TTL)
05	nOEF	enable output of port F (0:Output, 1:Input)
04	SELF	select port level F (0:NIM, 1:TTL)
03	nOEE	enable output of port E (0:Output, 1:Input)
02	SELE	select port level E (0:NIM, 1:TTL)
01	nOED	enable output of port D (0:Output, 1:Input)
00	SELD	select port level D (0:NIM, 1:TTL)

The lowest 7 bits control the mounted extension cards and are directly wired to the corresponding ports of the V1495 entity which are connected to the extension cards. These signals work only for the cards which have the opportunity of selecting their I/O direction and their logic level. The bits 8 to 12, corresponding to memory accesses, are explained in the following section. Bit 13 enables the usage of the additional EDM triggers' information, as explained in section 5.3.3.

Cosy register: The cosy register buffers information on the current COSY status. This information includes three bits representing the current energy of the beam, four bits notifying the spin state, one bit showing the status of the RF and four bits holding the Flattop status. Table 5.5 documents the coding of these twelve cosy status register bits. The cables transporting all this information are connected to the first twelve channels of port D of the V1495 board.

Table 5.5: *Coding of the cosy register.*

Bit	Content
11–08	Flattop status
07	RF on / off
06–03	spin state
02–00	energy bits

Readout registers: The first two bits of the REG_READOUTCOUNTERS control the scalers. The first bit drives the readout input port of the scalers entity. A rising edge of bit 1 causes a shift of the current scaler values to the output ports of the scalers entity. These shifted values feed all scaler registers readable at the associated addresses via the VME bus.

Setting the second bit to 1 generates a global reset of all scalers. The bits 2 to 31 have no functions.

Mask registers: The MASK0 to MASK28 registers are accessible in writing and reading mode. A writing access to these registers sets the input of the memory block, holding the masks to sift the kinematically allowed ring combinations, to the first 29 bits of the written words. These words are written to the memory if the enable write bit (RamWren), controlled via the register REG_CTRL, is set to 1. A reading access to the mask registers transfers the content of the current selected mask to the readout computer. This feature can be used for verifying if all masks are loaded correctly.

5.3.6 Memory to store the masks

The memory block, holding the masks for the coincidence of the rings, consists of four 841 bit wide words. Each word represents a 29×29 dimensional matrix for one energy range. Row number i of this matrix is the bit pattern used to mask ring number i in the coincRings entity.

The memory's input signals are one 841 bit wide data bus, two clocks, one 2 bit address signal and one write enable bit. The written mask registers feed the data input bus of the memory. The address bus selects one of the four words to read and to write. The mask, buffered in the data bus, is written to memory by a high write enable bit and a rising edge of clock0. Every rising edge of clock1 refreshes the output of the memory.

The firmware has two possibilities to select the address of the memory: one is to select the address via the VME bus, the second is to select the address via the energy of the COSY beam. This energy value is coded in the three energy bits connected to port D. Bit 12 of the control register switches between these two modes. A high bit selects the address saved in the control register; a low bit selects the three input channels of port D as address bits. The coding of the address, shown in table 5.6, is the same in both modes.

Table 5.6: *Memory address map.*

Value of the address bits	Selected mask
000	direct scaler mode
001	mask 1
010	mask 2
011	mask 3
100	mask 4

The selected 841 bit wide output is divided in 29 vectors. Each vector has a depth of 29 bit. The resulting vectors are the input masks of the coincRings entity.

6 Functionality test of the firmware

This chapter describes a test of the masks for all five energy ranges and a test of the classification in the four categories Up, Right, Down and Left. For these tests all discriminators, normally fed by the PMT signals, are set in remote mode. Where all channels of the discriminators can be individually activated by a computer. A square-wave signal with a frequency of 1 MHz, generated by a clock generator, feeds the inputs of all discriminators.

6.1 Test of the masks

To test the masks for the rings all discriminators, dedicated to the bars, are turned on. For each side of the detector (left and right) one discriminator, dedicated to one semiring, is turned on. All of the others are turned off. This configuration simulates two particles detected by EDDA. One particle is detected in the left side of the detector, the other one in the right side. Their two angles, θ_1 and θ_2, correspond to the ring numbers of the firing discriminators. For each combination of these two simulated semiring signals the channel numbers of the scalers for the left and right side of EDDA, which register a non-vanishing rate, are identified.

The results of these tests are printed in tabular form. Each column of the tables corresponds to one simulated signal in the right semirings of EDDA. Each row belongs to one signal in the left half rings of EDDA. The content of the table elements is the active scaler channel number. These tables are plotted above the masks, determined in chapter 4, for each of the four energy ranges. The resulting plots are figures 6.1 to 6.4.

Selecting of one of the four masks generates entries only for the two semirings which fulfil the kinematic relation of the two angles θ_1 and θ_2 (equation 4.1). For instance, selecting mask 1 and firing the semiring right 20 will lead to an active scaler channel 22 if one of the semirings left 5 to 11 is also on.

The evaluation of the tables points out a correct wiring of the discriminators, the V1495 board and the VME scaler module. The scaler channels 0 to 15 belong to the semirings left 14 to 29 as expected. Active semirings right 14 to 29 produce signals

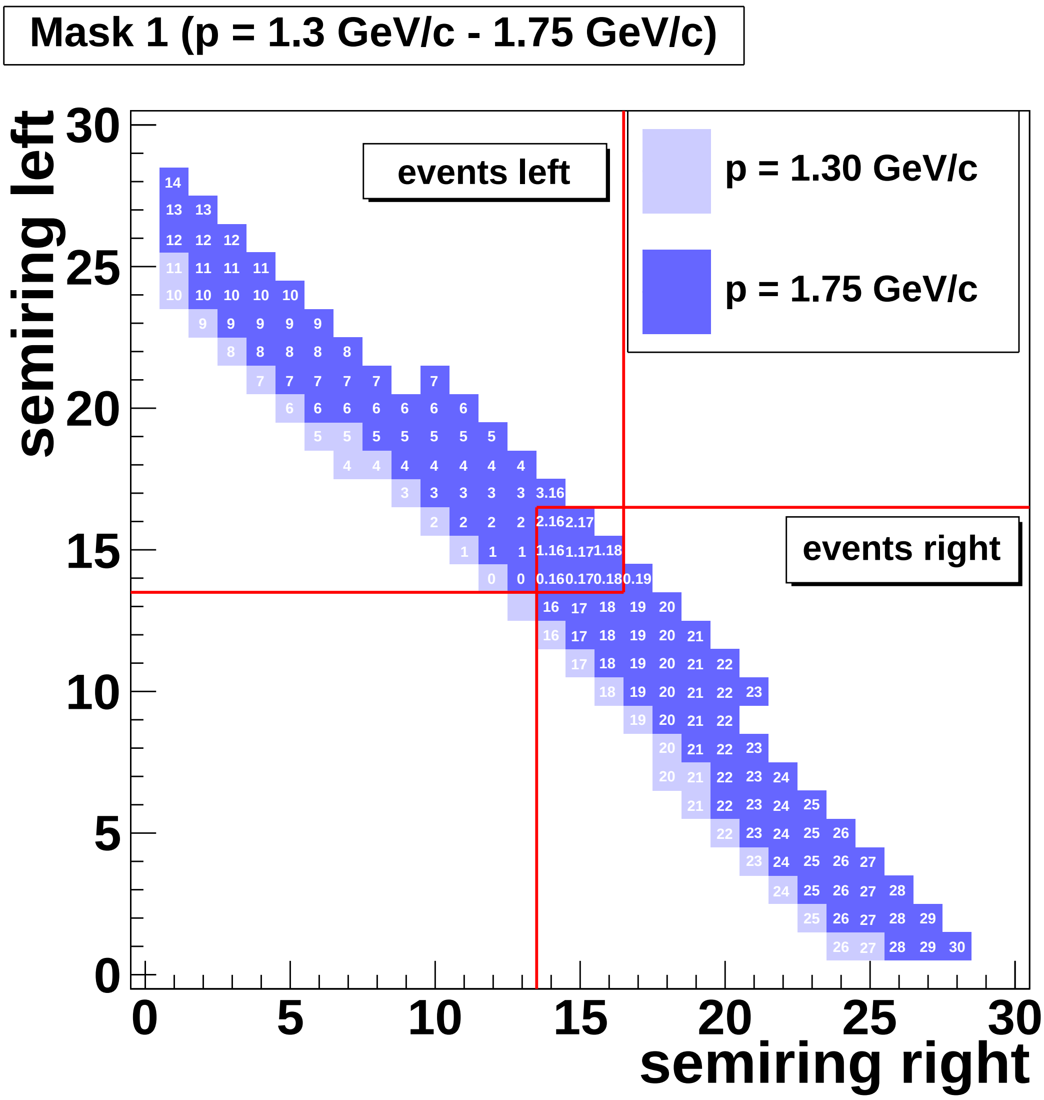

Figure 6.1: *Active scalers for the selected mask 1.*

in the scaler channels 16 to 31. These relations between the scalers and the semirings depict a right cabling of the modules and a correct readout of the scalers.

The analysis of the entries in the tables, recorded with the selected masks 1 to 4, shows the firmware sorting out the kinematically allowed combinations of the two angles, θ_1 and θ_2, of the two particles. All in all, the entity to combine the signals of the left and right semirings screens the kinematically allowed events.

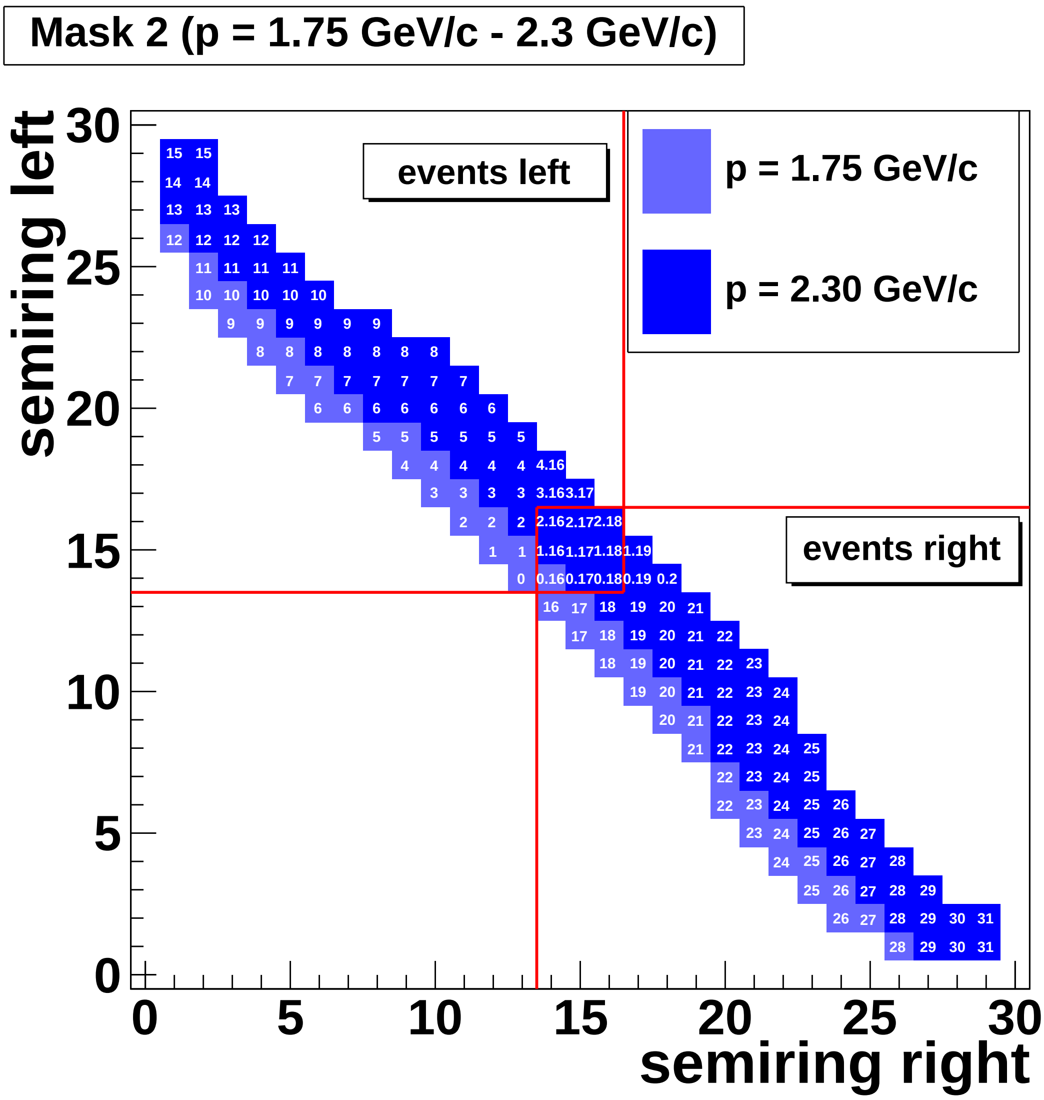

Figure 6.2: *Active scalers for the selected mask 2.*

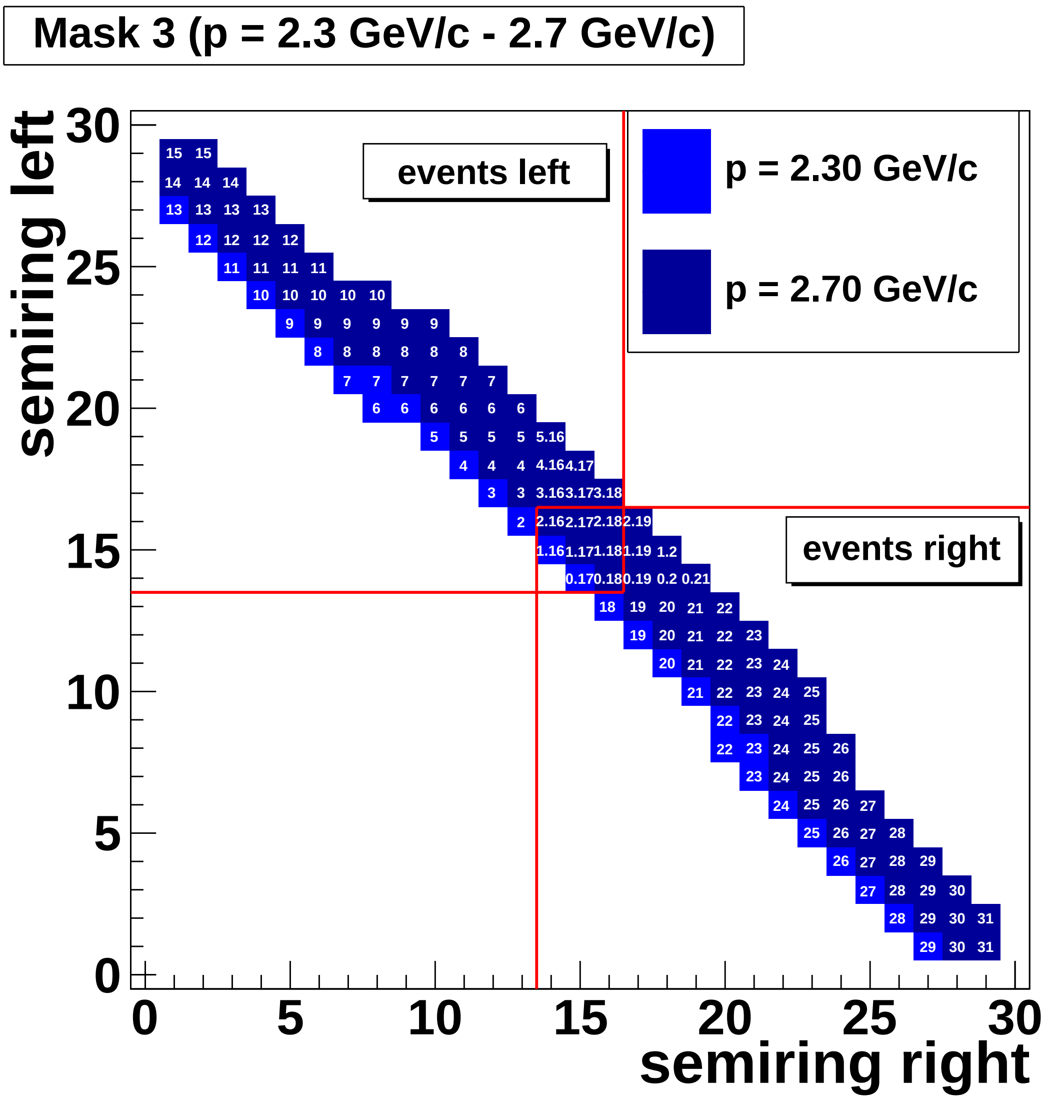

Figure 6.3: *Active scalers for the selected mask 3.*

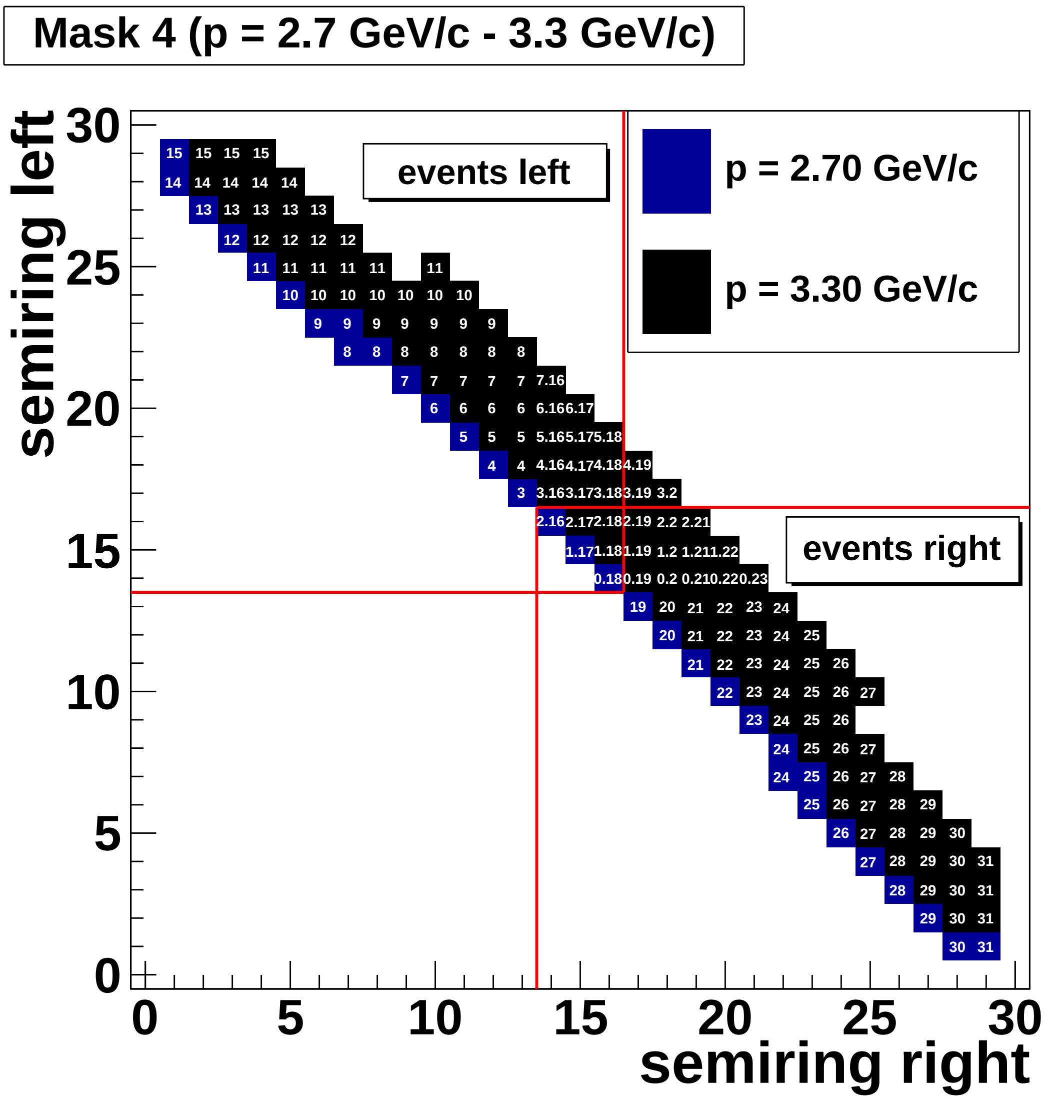

Figure 6.4: *Active scalers for the selected mask 4.*

6.2 Event classification check

Additionally to the signals' test of the rings, the processing of the bar signals is checked. With the help of the bar signals, a classification of the recorded event in one of the categories Up, Right, Down and Left is possible. The test of the classification is done for two different event signatures in the rings: one for the direct scaler mode and one for the mode with mask 1 selected. Table 6.1 lists the settings used for the half ring discriminators. The combination of the semirings 10 and 16 is chosen

Table 6.1: *Half ring signal settings for the bar test.*

Setting	Simulated event	HRDs on	HRUs on
1	elastic scattered proton left	16	10
2	elastic scattered proton right	10	16

as they fulfil the kinematic coincidence for mask 1. Therefore, the event passes the coincRings entity and reaches the entity to combine the semiring signals and the bar signals. The combination of two semiring signal settings with two modes (direct scaler, mask 1) causes four different configurations to be tested.

For each test the discriminators of the semirings are set up as described in table 6.1. Two of the discriminators, corresponding to the bars, are on. For each possible combination of these two discriminators the active scalers are identified. These scalers and their acronyms, used in the following, are:

RR	Ring-Right (only rings)
RL	Ring-Left (only rings)
U	Up
R	Right
D	Down
L	Left

The scalers, Ring-Right and Ring-Left, use the signals of the rings only. The other four scalers use the combined information of the rings and the bars. The two scalers, Ring-Right and Ring-Left, are the external VME scalers fed by the output of the coincRings entity. The other four ones are the scalers implemented in the firmware.

The identified active scalers are illustrated in one table for each setting. Every position in the table corresponds to one specific combination of two firing bars. Each row corresponds to one firing bar discriminator. The columns define the second firing bar discriminator. The firing bars and the active scalers for the coloured table elements are plotted in a profile of the EDDA detector to explain the positions of the active rings and bars.

6.2.1 One scattered proton in the left EDDA region

A run of the half ring discriminators with setting 1 and a selection of the direct scaler mode lead to the results listed in table 6.2.

Table 6.2: *Results for running the half rings with setting 1 and a selected direct mode.*

	bar 0	bar 1	bar 2	bar 3	bar 4	bar 5	bar 6	bar 7
bar 0	RL	RL	RL	RL	D RL	L RL	L RL	U RL
bar 1	RL	RL	RL	RL	D RL	L RL	L RL	U RL
bar 2	RL	RL	RL	RL	D RL	L RL	L RL	U RL
bar 3	RL	RL	RL	RL	D RL	L RL	L RL	U RL
bar 4	D RL	D RL	D RL	D RL	D RL	L D RL	L D RL	U D RL
bar 5	L RL	L RL	L RL	L RL	L D RL	L RL	L RL	L U RL
bar 6	L RL	L RL	L RL	L RL	L D RL	L RL	L RL	L U RL
bar 7	U RL	U RL	U RL	U RL	U D RL	L U RL	L U RL	U RL

In all table elements one entry is RL so the scaler Ring-Left is independent of the signals in the bars, as desired. The Down scaler is only running for a signal in bar 4, and not for a signal in bar 3, as the right semiring is without a signal. A signal in bar 5 or bar 6 drives the Left scaler. The Up scaler is triggered by a signal in bar 7. Bar 0 does not influence the Up scaler since the right semiring is off.

Figure 6.5 picks up the coloured elements of table 6.2. The drawing shows the geometric positions of the bars and the semirings. All scalers are sketched around the detector. The angular range of the scalers represents the angular range which is assigned to the scalers. The firing bars and half rings are coloured in orange. The identified, active scalers are shaded in green. This figure clarifies the connection between the firing detector elements and the active scalers:

(a) Active semiring left fires the scaler Ring-Left. The coincidence of semiring left and bar 4 triggers the scaler Down.

(b) Active semiring left fires the scaler Ring-Left. The coincidence of semiring left and bar 6 triggers the scaler Left. The scaler Down is triggered by bar 4 and semiring left.

Changing the mode from direct mode to mask 1 results in table 6.3. In this mode, the scalers including the bar signals are active if opposite bars fulfil a coincidence. Therefore, the Down scaler is only running if bar 0 and bar 4 are firing. The Left scaler is active if bar 1 and bar 5 or bar 2 and bar 6 are active simultaneously. A

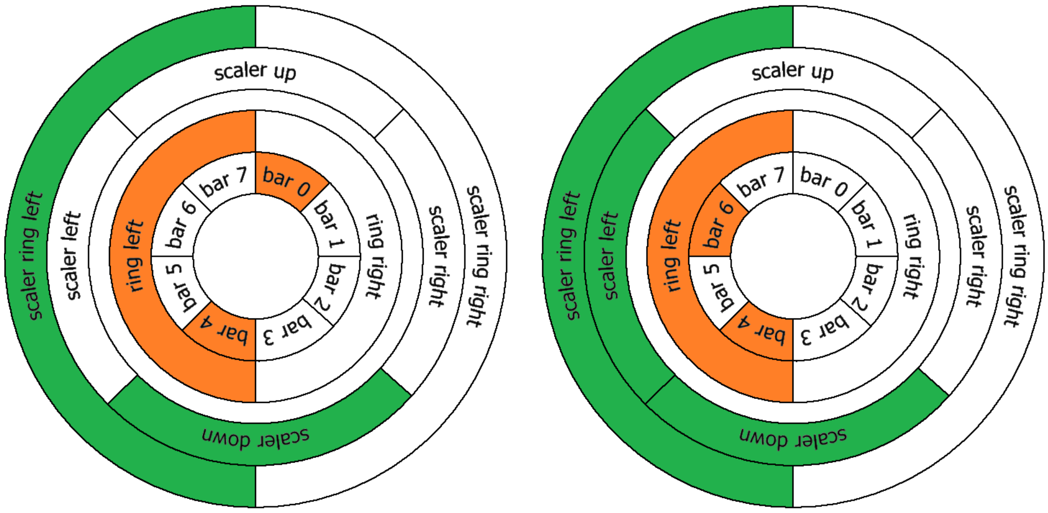

(a) *Firing discriminators: bar 0, bar 4 and semiring left.*

(b) *Firing discriminators: bar 4, bar 6 and semiring left.*

Figure 6.5: *Example of active scalers for setting* 1 *in direct scaler mode.*

coincidence of bar 3 and bar 7 drives the Up scaler. The scaler Ring-Left is working in the same way as in the direct scaler mode.

Table 6.3: *Results for running the half rings with setting 1 and selecting mask 1.*

	bar 0	bar 1	bar 2	bar 3	bar 4	bar 5	bar 6	bar 7
bar 0	RL	RL	RL	RL	D RL	RL	RL	RL
bar 1	RL	RL	RL	RL	RL	L RL	RL	RL
bar 2	RL	RL	RL	RL	RL	RL	L RL	RL
bar 3	RL	RL	RL	RL	RL	RL	RL	U RL
bar 4	D RL	RL	RL	RL	RL	RL	RL	RL
bar 5	RL	L RL	RL	RL	RL	RL	RL	RL
bar 6	RL	RL	L RL	RL	RL	RL	RL	RL
bar 7	RL	RL	RL	U RL	RL	RL	RL	RL

The active scalers for the coloured cells of table 6.3 are sketched in figure 6.6:

(a) Active semiring left fires the scaler Ring-Left. The coincidence of bar 0, bar 4 and semiring left triggers the Down scaler.

(b) Active semiring left fires the scaler Ring-Left. The scalers counting the bar signals are all inactive, as firing bar 4 and bar 6 does not fulfil the coincidence of opposite bars.

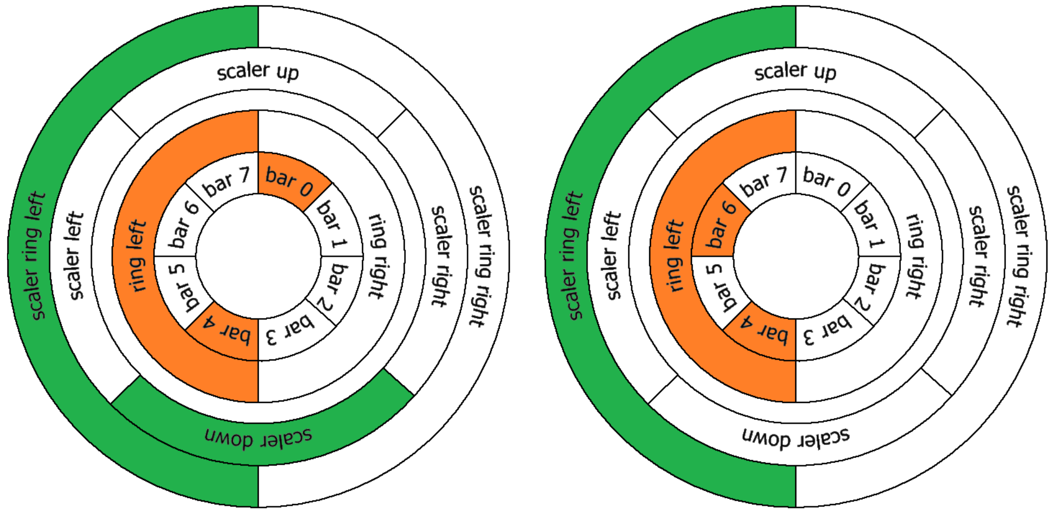

(a) *Firing discriminators: bar 0, bar 4 and semiring left.*

(b) *Firing discriminators: bar 4, bar 6 and semiring left.*

Figure 6.6: *Example of active scalers for setting* 1 *and selected mask* 1*.*

6.2.2 One scattered proton in the right EDDA region

The test of the bar signal processing in combination with a simulated proton in the right EDDA region operates in a similar way. The semiring discriminators work in setting 2. Two out of the eight bar discriminators are on. For each combination of bars the active scalers are recorded and printed in table 6.4 for the direct mode and in table 6.5 for mask 1. The scaler Ring-Right is active in both modes independent

Table 6.4: *Results for running the half rings with setting 2 and selecting the direct mode.*

	bar 0	bar 1	bar 2	bar 3	bar 4	bar 5	bar 6	bar 7
bar 0	U RR	R U RR	R U RR	U D RR	U RR	U RR	U RR	U RR
bar 1	R U RR	R RR	R RR	R D RR	R RR	R RR	R RR	R RR
bar 2	R U RR	R RR	R RR	R D RR	R RR	R RR	R RR	R RR
bar 3	U D RR	R D RR	R D RR	D RR	D RR	D RR	D RR	D RR
bar 4	U RR	R RR	R RR	D RR	RR	RR	RR	RR
bar 5	U RR	R RR	R RR	D RR	RR	RR	RR	RR
bar 6	U RR	R RR	R RR	D RR	RR	RR	RR	RR
bar 7	U RR	R RR	R RR	D RR	RR	RR	RR	RR

of the signals in the bars. In direct mode the scaler Up is driven by bar 0. The scaler Right is active if bar 1 or bar 2 are firing. An active bar 3 leads to a counting scaler Down. The other bars produce no signal in the scalers because the left semiring is off.

Table 6.5: *Results for running the half rings with setting 2 and selecting mask 1.*

	bar 0	bar 1	bar 2	bar 3	bar 4	bar 5	bar 6	bar 7
bar 0	RR	RR	RR	RR	U RR	RR	RR	RR
bar 1	RR	RR	RR	RR	RR	R RR	RR	RR
bar 2	RR	RR	RR	RR	RR	RR	R RR	RR
bar 3	RR	RR	RR	RR	RR	RR	RR	D RR
bar 4	U RR	RR	RR	RR	RR	RR	RR	RR
bar 5	RR	R RR	RR	RR	RR	RR	RR	RR
bar 6	RR	RR	R RR	RR	RR	RR	RR	RR
bar 7	RR	RR	RR	D RR	RR	RR	RR	RR

Figure 6.7 illustrates the coloured scenarios of table 6.4 in direct mode with a firing right semiring. In scenario (a) the bars 0, 4 and the right semiring are on. Therefore, the scaler Up and the scaler Ring-Right are counting non-zero rates. In case (b) only bar 0 and the right half ring are on. This leads to active scalers Right and Ring-Right.

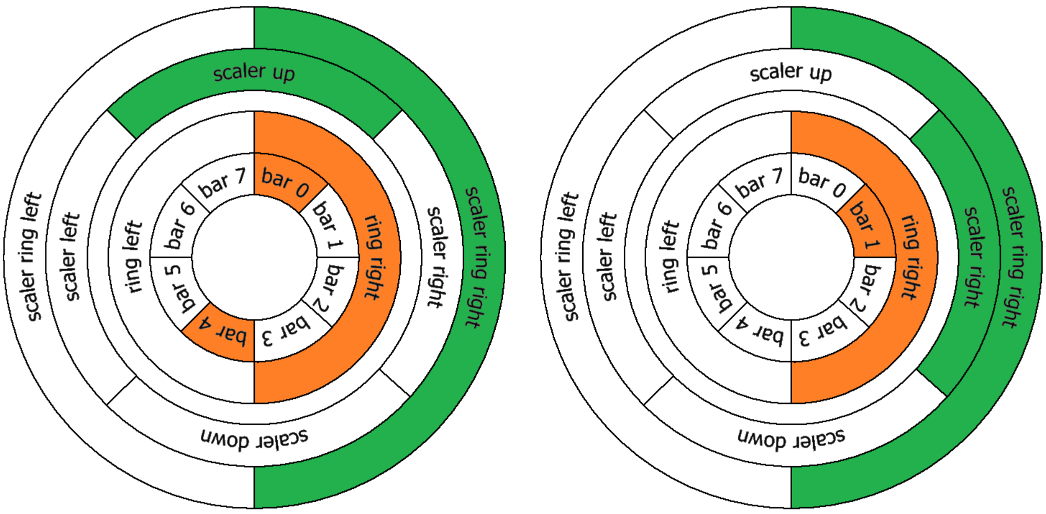

(a) *Firing discriminators: bar 0, bar 4 and semiring right.* (b) *Firing discriminators: bar 1 and semiring right.*

Figure 6.7: *Example of active scalers for setting 2 in direct scaler mode.*

In the mode with a selected mask only signals in opposite bars drive the scalers. As a consequence the scalers Up, Right and Down are just active for signals in the bar's combinations bar 0 and bar 4, bar 1 and bar 5, bar 2 and bar 6; bar 3 and bar 7.

Figure 6.8 shows the same firing bars and semirings for mask 1 as for the direct mode. In this case the processing of the bar signals requests a signal in opposite bars.

In figure 6.8(a) the opposite bars 0 and 4 are active, thus the same scalers as in the direct mode are on: active semiring right fires the scaler Ring-Right. The coincidence of bar 0, bar 4 and semiring right triggers the Up scaler.

In contrast to the direct scaler mode a single active bar leads to inactive scalers (figure 6.8 (b)): active semiring right fires the scaler Ring-Right. The scalers, counting the bar signals, are off as firing only bar 1 does not fulfil the coincidence of opposite bars.

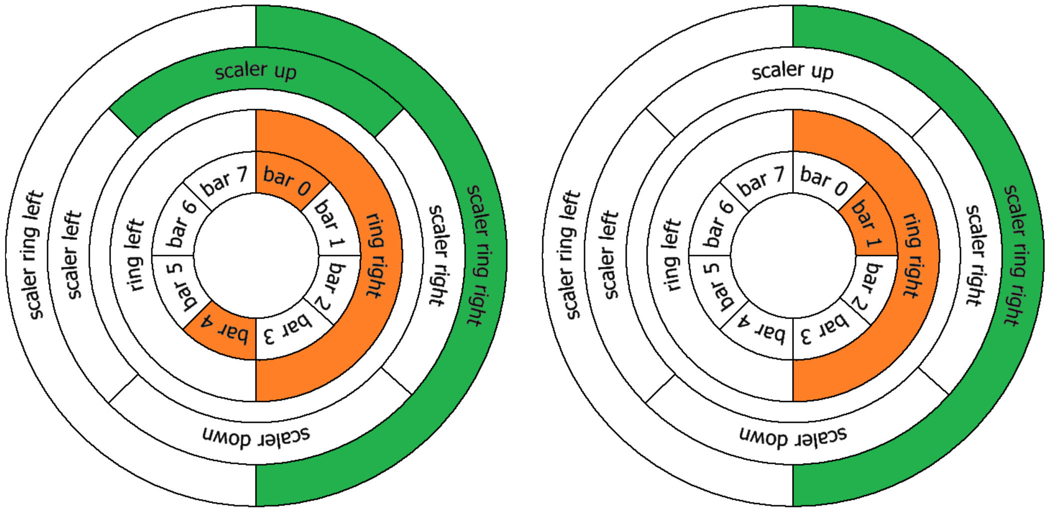

(a) *Active discriminators: bar 0, bar 4 and semiring right.*

(b) *Active discriminators: bar 1 and semiring right.*

Figure 6.8: *Example of active scalers for setting* 2 *and selected mask* 1.

6.2.3 Classification check conclusion

The test with the bar and the semiring signals demonstrates that the classification of the events recorded in the four sections of EDDA is working properly. Only with the information of the semirings, the events can be classified in the categories Ring-Left and Ring-Right. The addition of the bar signals leads to a correct assignment to the four categories Up, Left, Down and Right. The comparison of the results recorded in direct mode and with active mask 1 illustrates the correct behaviour of the coplanar trigger implemented in the firmware.

6.3 Functionality test summary

Recapitulating, the kinematic trigger, considering the two angles θ_1 and θ_2, and the coplanar trigger, regarding $\Delta\phi = 180°$, operate properly. The four masks are transferred correctly and saved in the memory. The load the selected mask and the application of the mask to the semiring signals function correctly.

The recording of the events in the categories Up, Right, Left and Down with respect to the scattering angle of the forward scattered particle leads to an angle-dependent determination of the asymmetries Left-Right and Up-Down. Due to these asymmetries the determination of the polarisation, with respect to the angle-dependent analysing power, is possible.

7 Beamtime July 2013

The programmed V1495 board was tested for the first time in the July beamtime[13] of the EDM experiment at COSY. The aim of this test was a comparison of the old and the new electronics. For this purpose the two systems were working simultaneously. The test contains the semirings only, therefore the bars were not connected to the V1495 module. The entity including the bar signals was switched off and the implemented Left-Right scaler was directly connected to the output of the kinematic coincidence entity. In this configuration the implemented scalers and the external VME scalers are driven by the same signals, so a comparison of these two scalers proves the correct function of the implemented scalers. A detailed description of the experimental setup and the installation is given in section 7.1. The ensuing section 7.2 describes the results of the comparison.

7.1 Installation of hardware

During the beamtime, the board V1495 and one VME scaler (SIS3820) were installed in a VME crate. This crate and the installed boards are accessible via the edda03 computer which generates the data stream to the DAQ system. Figure 7.1 is a schematic overview of the cabling of the PMT signals, the discriminators and all modules.

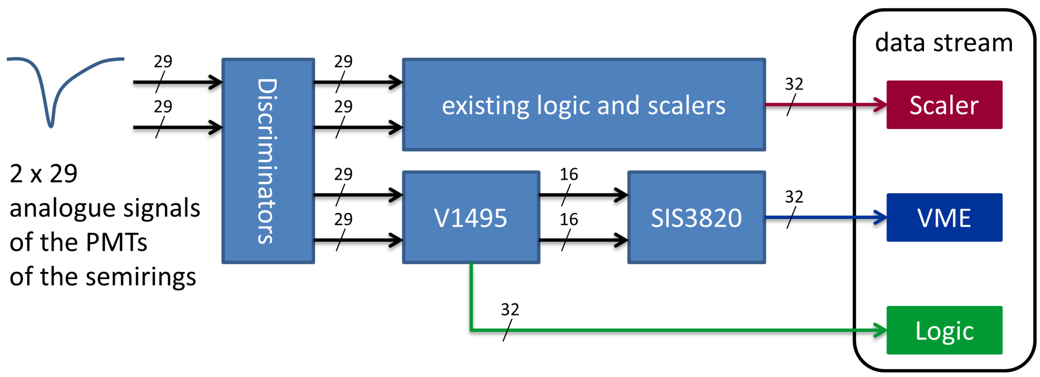

Figure 7.1: *Schematic overview of the module wiring for the July beamtime.*

[13] 4th of July to 12th of July 2013

The analogue signals out of the PMTs of the 58 semirings are connected to discriminators. Each of the discriminators has two outgoing ports. One port is connected to the existing logic. The second one is wired to the ports A and B of the V1495 logic module. The outgoing port F, holding the signals to be counted, is linked to the VME scaler SIS3820. The rates counted by the V1495 and the SIS3820 are read out via the VME crate. These rates are added to the existing data stream. The rates counted by the V1495 logic module are named Logic, the rates measured by the VME scaler are named VME. The data, labelled Scaler, correspond to the existing logic.

7.1.1 Implementation of the new modules into the existing DAQ

The software interface to control the readout of the EDDA detector is shown in figure 7.2. A click on the init button initialises all modules. During this initialising process the four masks, filtering the elastic events, are loaded in the memory of the programmed FPGA. Additionally, all scalers are cleared. By clicking the start button the run starts and all scaler values are cleared. During a run the scalers are readout with a frequency of 1 kHz. All VME commands, needed to control the FPGA, are implemented in the DAQ software files. A stop process does not need any functions concerning the FPGA.

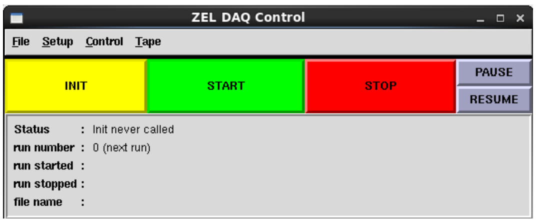

Figure 7.2: *EDDA DAQ software interface.*

7.2 Analysis of the data

This section presents the results of the first measurement with the V1495 logic module.

The analysis consists of three main parts:

- Estimation of the correlation between all scaler modules.
- Evaluation of the ratio of the scalers per semiring with respect to the estimated coefficient of correlation.
- Measuring of the Left-Right asymmetry with all scalers for all semirings.

7.2.1 Run setup

During the beamtime, COSY was filled with unpolarised protons with a momentum of 485 GeV/c. Due to the low momentum of the protons the V1495 module worked in direct scaler mode and the masks were not used. The beam was cooled in the first 60 seconds of each cycle. After the cooling period, the beam was horizontally heated and steered onto the carbon target. Thus the elastic scattering of the protons on the nucleus of the carbon target took place. The data taking period, 60 seconds, started synchronously to the heating of the beam. 20 seconds after the start of the data taking period, a vertical heating of the beam began to increase the extraction of the particles.

The analysed data were taken in run 2074, consisting of ten cycles. The first nine cycles lasted 170 seconds which led to a data taking time of 60 seconds per cycle. The last cycle took only 70 seconds which is equal to a data taking time of 10 seconds.

7.2.2 Spectra of the scalers

Each of the lowest 16 semirings is connected to three scalers which should count the same rate. Typical spectra of one semiring, measured by all three scalers, are shown in figure 7.3. The histograms contain the sum of the counted signals of all cycles in

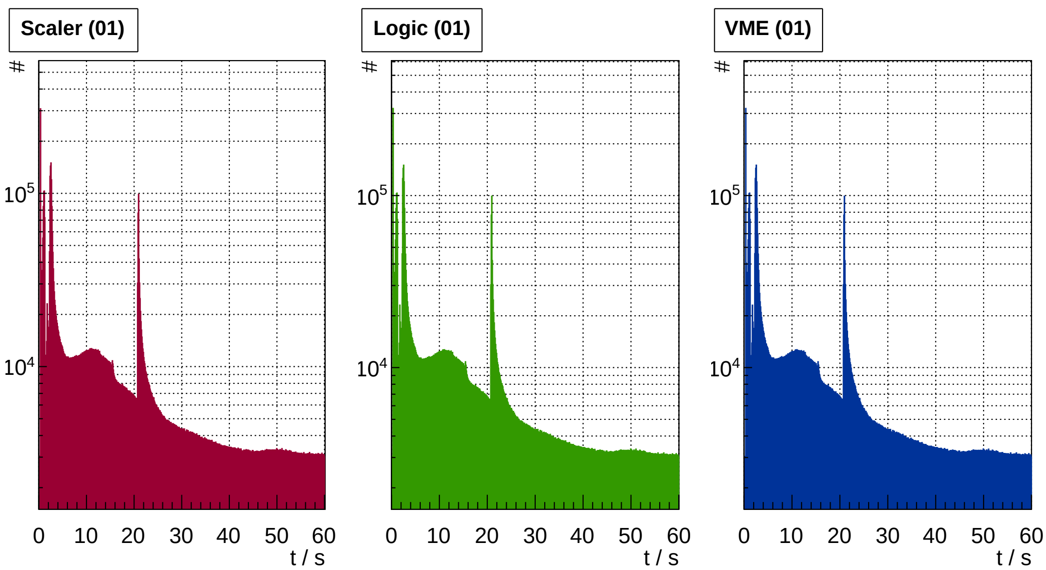

Figure 7.3: *Spectra of channel 01 (semiring left 15) for all three scalers.*

time intervals of 1 ms. The first peaks represent the beginning of the extraction, when the beam is moved towards the target. The peak close to 20 seconds corresponds to the starting of vertical heating. The first 10 seconds contain the sum of all cycles of the run. The last 50 seconds include only the sum of the first nine cycles' rates, as the last cycle stops after the first 10 seconds of data taking. This causes the step in the spectra at 10 seconds.

Almost all spectra of all channels show the same pattern, only channel number 11 which corresponds to the left semiring number 25, looks different. Its spectrum, measured by all scalers, is shown in figure 7.4. This spectrum is almost flat except for the step at 10 seconds. Obviously this channel is not working correctly, the spectrum probably consists just of electronic noise.

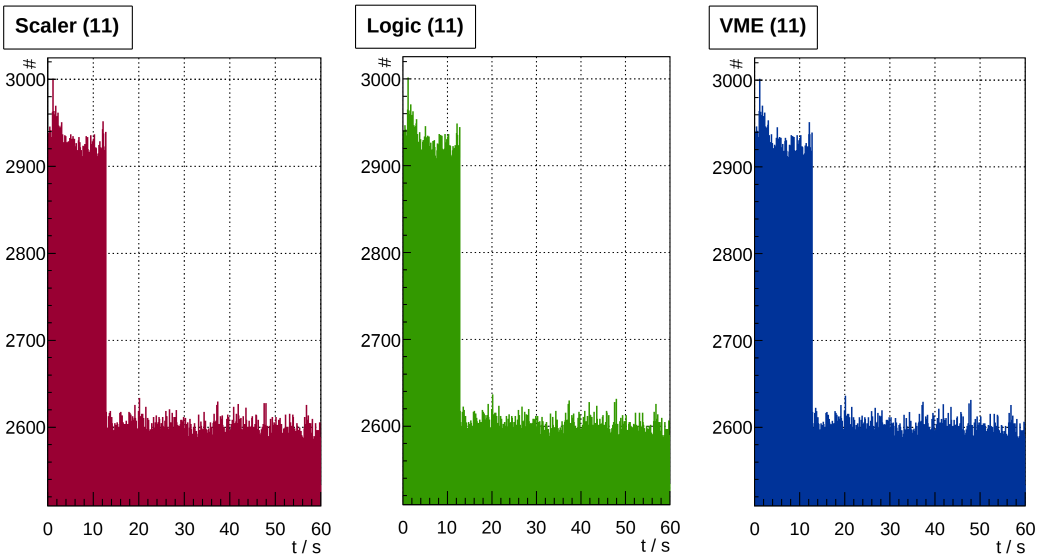

Figure 7.4: *Spectra of channel 11 (semiring left 25) for all three scalers.*

7.2.3 Fourier transformation of the spectra

To find systematic effects in the spectra the spectra are Fourier transformed. The resulting frequency spectra for the channels 01 and 11 are shown in figures 7.5 and 7.6. The spectra of all other channels are similar to the one of channel 01. The Fourier spectra of the different scalers for each channel look identical, indicating that there is no systematic effect in one of the two electronic systems. The spectra of channel 01 contain peaks at 100 Hz with corresponding harmonics. Beside these peaks there are further peaks at 50 Hz with corresponding harmonics. The spectra of channel 11 show the same 100 Hz and 50 Hz peaks. They are of the same size as the ones in the spectra of channel 01. The background is flat with an amplitude of 10^3. This is 2 to 3 magnitudes lower than the one of channel 01. In addition to the 100 Hz artefacts, peaks at the harmonics of 50 Hz appear. The comparison of the two frequency spectra suggest that channel 11 measures only the electronic noise and not the signals of the connected PMT. The 50 Hz problem is seen in many COSY

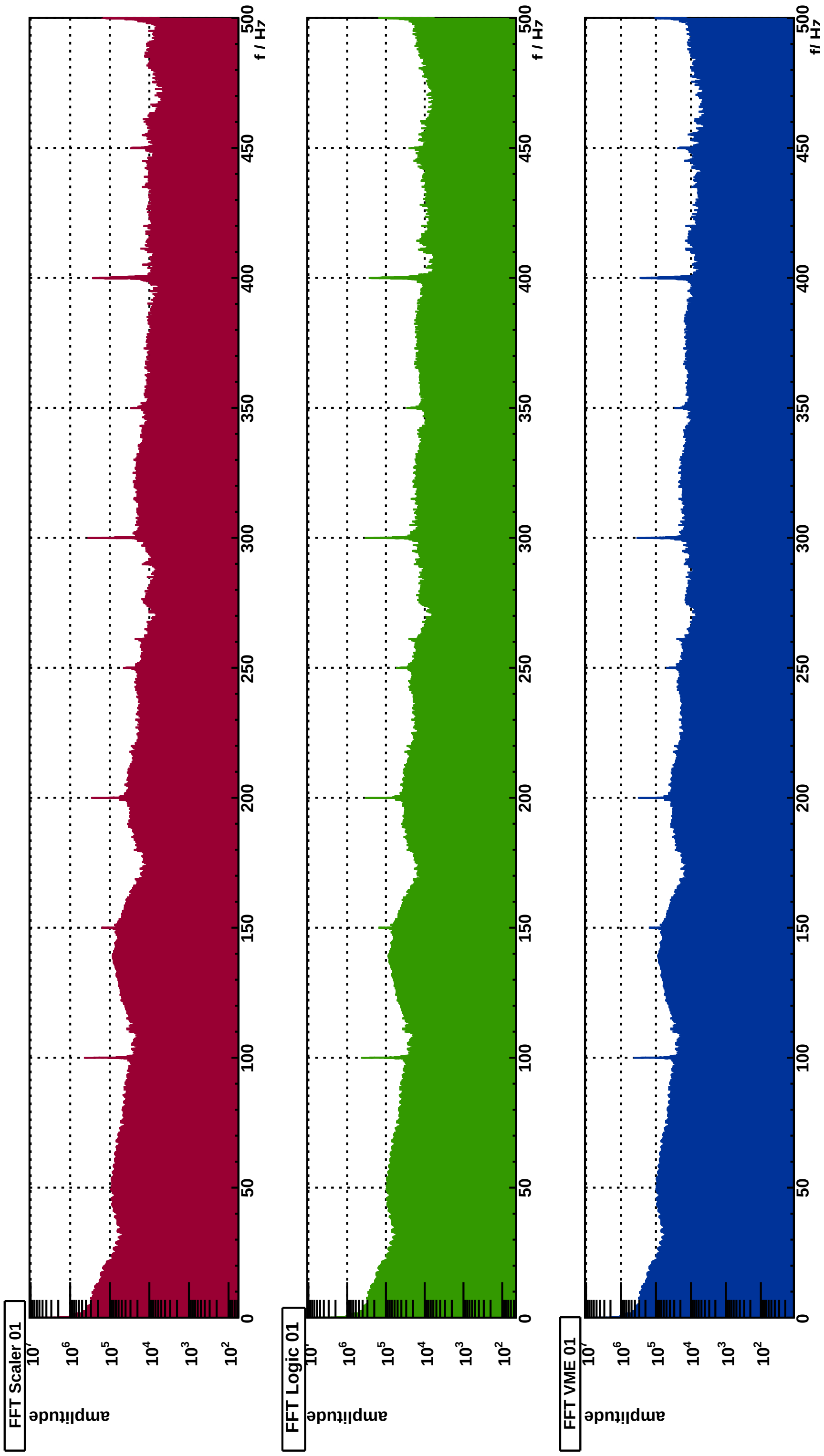

Figure 7.5: *Frequency spectra of channel 01.*

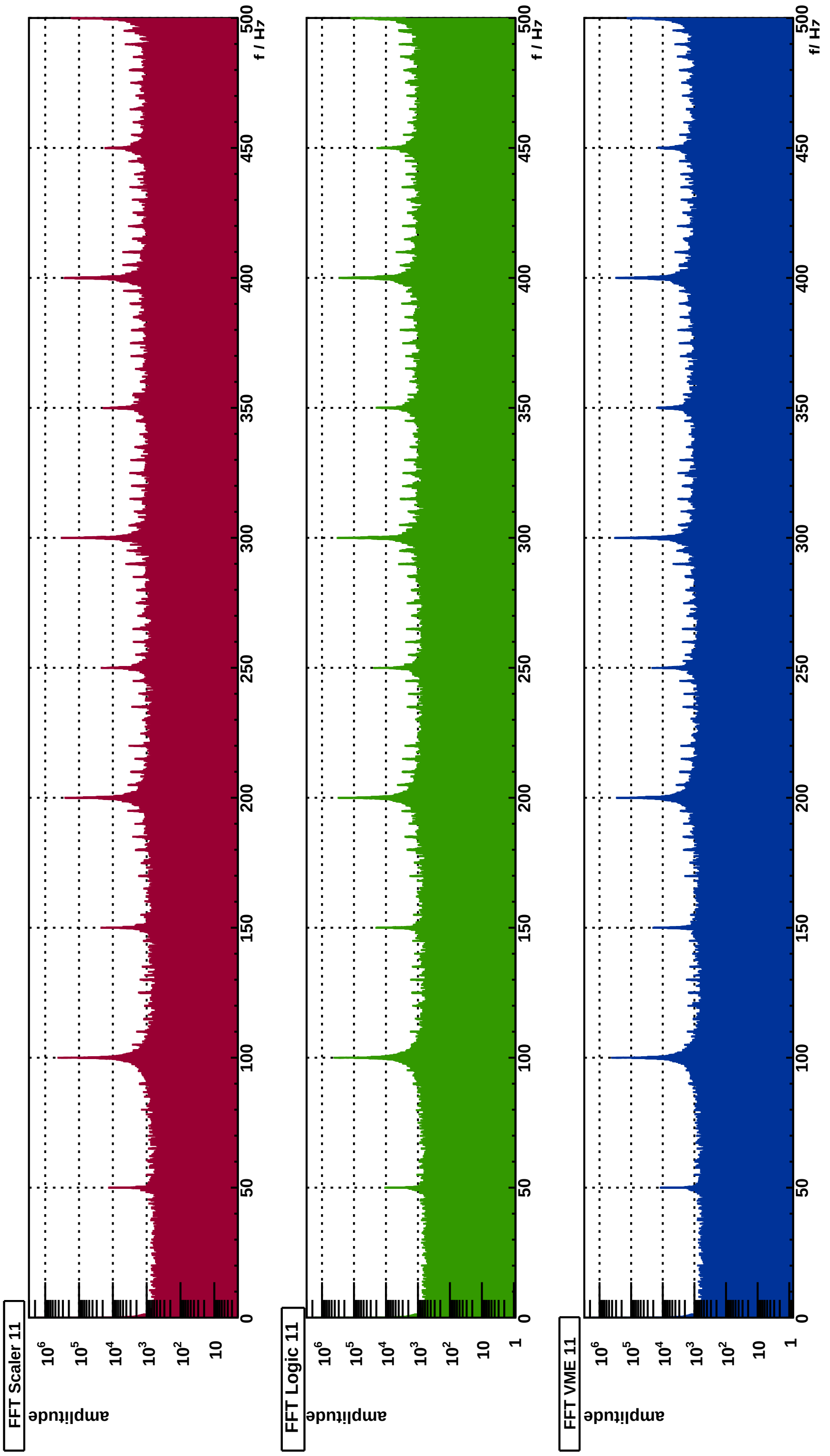

Figure 7.6: *Frequency spectra of channel 11.*

experiments and still under investigation. The source of the 100 Hz peaks was found after the beamtime. The fan-in/fan-out module, used to feed all discriminators with the test pulses, produces a rectangular signal with a frequency of 100 Hz. During the beamtime the test pulses are off but the module is switched on and connected to the discriminators. This setup feeds the 100 Hz artefact into the signals. A deeper investigation showed, that unplugging the fan-in/fan-out module removes the 100 Hz signal. Therefore this module will be unplugged during the next measurements with the EDDA detector.

7.2.4 Correlations between the three scalers

Each of the channels is counted by three scalers. Therefore these scalers are statistically dependent. This causes a non-vanishing correlation coefficient ρ. It has to be respected in all results and is calculated by using

$$\rho_{x,y} = \frac{\sum_{i=0}^{N} N \cdot x_i \cdot y_i - \sum_{i=0}^{N} x_i \cdot \sum_{i=0}^{N} y_i}{N^2 \cdot \sigma_x \cdot \sigma_y}. \tag{7.1}$$

The variables x_i and y_i are the values of the scalers x and y in the 1 ms long time interval i. The values σ_x and σ_y are the RMS[14] values of the scaler value distributions. The number of recorded intervals is referred to as N. A graphical illustration of the correlation between the three scalers of semiring left 15 is presented in figure 7.7. Each point in the scatterplot corresponds to the scaler values of 1 ms long time interval. The abscissa presents the first mentioned scaler of each point cloud, the ordinate the second one. The depicted coefficients of correlation are calculated by using formula 7.1. The three shown correlation coefficients are calculated for all scalers of every semiring. These coefficients are used in the error estimation of the scaler ratios (cf. next section).

7.2.5 Ratios of all scalers

The correct work of all scalers is verified by analysing the ratios of the scalers of one channel for each time interval. For right working scalers the ratios are expected to be 1. Assuming N_1 and N_2 as the scaler values in one time interval with the corresponding errors $\sigma_{N_i} = \sqrt{N_i}$, the ratio is calculated with

$$r = \frac{N_1}{N_2}. \tag{7.2}$$

[14]Root Mean Square

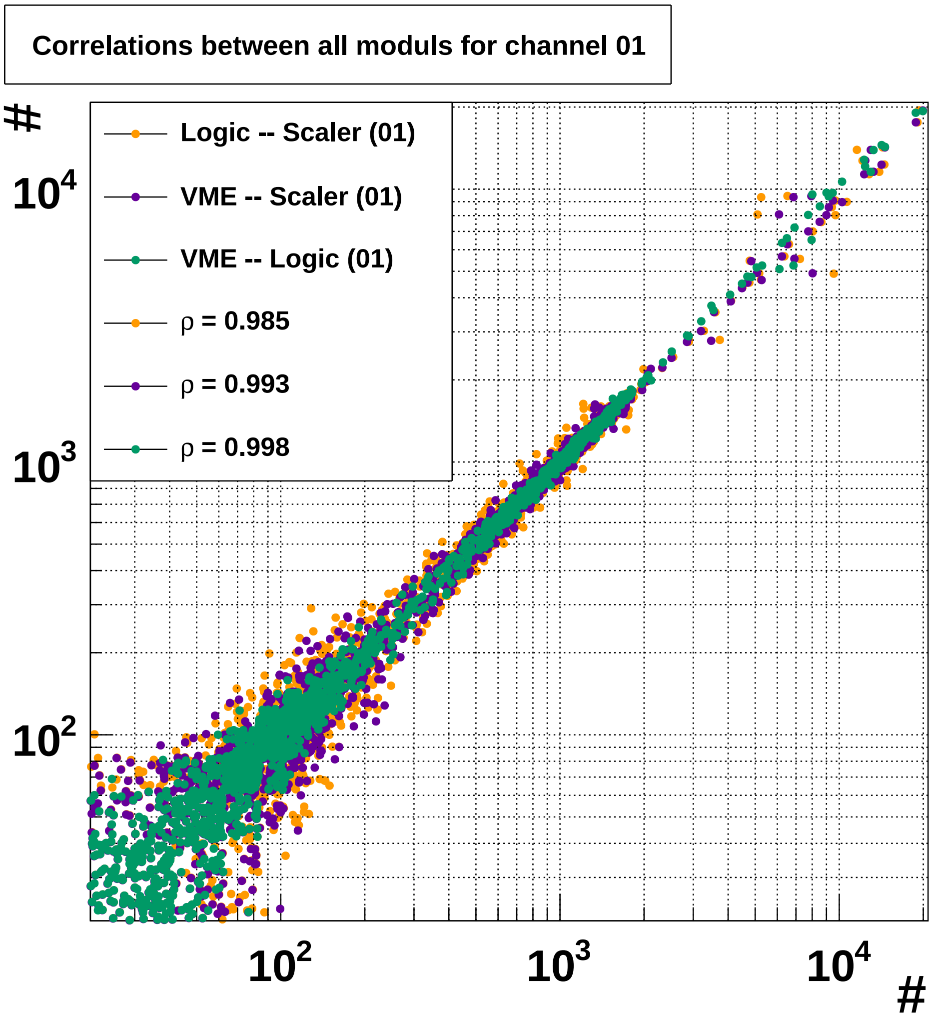

Figure 7.7: *Scatterplot of the three scalers corresponding to channel 01 (semiring left 15).*

The error propagation with respect to the correlation between the two scaler values results in formula (7.5). On the assumption that the rates are Poisson distributed the statistical error for each counted rate N_i is $\sigma_{N_i} = \sqrt{N_i}$.

$$\sigma_r^2 = \left(\frac{\mathrm{d}r}{\mathrm{d}N_1} \cdot \sigma_{N_1}\right)^2 + \left(\frac{\mathrm{d}r}{\mathrm{d}N_2} \cdot \sigma_{N_2}\right)^2 + 2\frac{\mathrm{d}r}{\mathrm{d}N_1}\frac{\mathrm{d}r}{\mathrm{d}N_2} \cdot \mathrm{cov}\,(N_1, N_2) \tag{7.3}$$

$$= \frac{\sigma_{N_1}^2}{N_2^2} + \frac{N_1^2 \cdot \sigma_{N_2}^2}{N_2^4} - 2\frac{N_1}{N_2^3} \cdot \mathrm{cov}\,(N_1, N_2) \tag{7.4}$$

$$= \frac{N_1}{N_2^2} + \frac{N_1^2}{N_2^3} - 2\frac{N_1}{N_2^3} \cdot \sqrt{N_1 N_2} \cdot \rho_{N_1,N_2} \tag{7.5}$$

To get one value describing the ratio of two scalers, the calculated ratios are averaged over time. The averaging starts at 3 seconds to eliminate rate artefacts at the beginning of the beam extraction and ends with the end of the data taking period.

To cross check the right estimation of the errors a pull distribution for every averaged ratio is generated. This is done by filling the calculated pull values (formula (7.6)) for every time bin in one histogram.

$$pull = \frac{\overline{r} - r_i}{\sigma_{r_i}} \tag{7.6}$$

The calculation of the ratio for each combination of the scalers and for each channel results in 3×32 graphs illustrating the ratio over time.

These graphs are exemplarily discussed for semiring left 15. Figures 7.8, 7.10 and 7.12 show the corresponding plots. The first figure documents the comparison of the two new scalers. The other two plots compare the old scaler with one of the new ones. The top left plot of each figure contains the two compared spectra. One spectrum is the filled histogram, the other one is marked above with filled dots. The figures 7.9, 7.11 and 7.13 summarize the results for all channels.

The calculated ratio of these two scalers is plotted in the lower chart. The entries in this graph fluctuate around the calculated mean value. The alternating pattern of these fluctuations is caused by timing effects during the readout process. The scalers are readout one after another, therefore the rates vary. Calculating the average over several time bins compensates this effect. At the beginning of the extraction the effect is very large as the rate itself fluctuates. The calculated mean is indicated by a red straight line. The value and the error of the resulting mean are given in the right legend.

The pull distribution is plotted in the bottom-right corner. A right calculation of the mean and a correct estimation of the errors lead to a Gaussian pull distribution with mean 0 and a width of 1. The mean and the RMS of the pull distribution are also given in the legend mentioned before.

Comparison between Logic and VME scalers

Figure 7.8 shows the ratio of the Logic and VME scalers of channel 01. The calculated mean 1.0000 ± 0.0001 corresponds to an expected value of 1. The given parameters of the pull distribution suggest good error estimations.

The mean values for the ratios of the two scalers, Logic and VME, are plotted in figure 7.9 for all 32 channels. Almost all data points are compatible with 1, only channel 0 is about $5\,\sigma$ larger. The big error bar of channel 11 arises from the described measuring error of channel 11 (only electronic noise). All in all, the implemented scalers function properly.

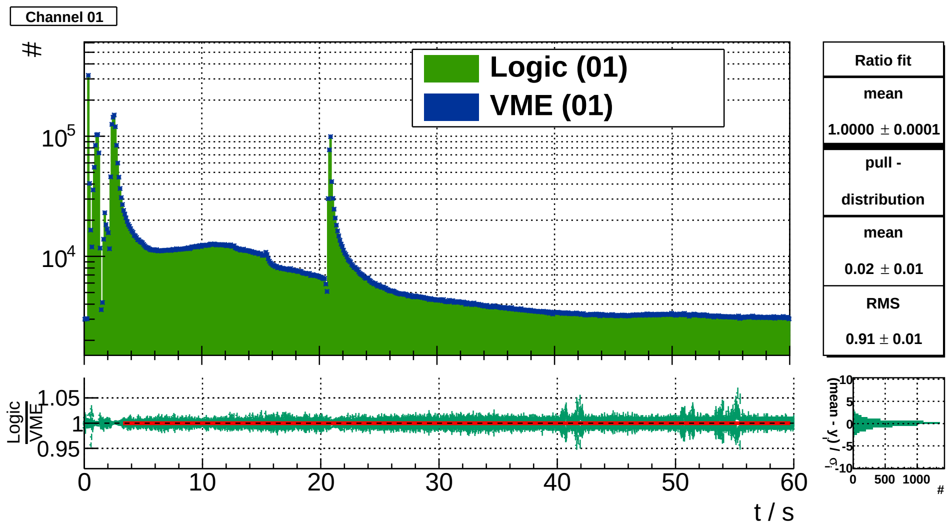

Figure 7.8: *Calculated ratio over time for the two scalers, Logic and VME, of channel 01.*

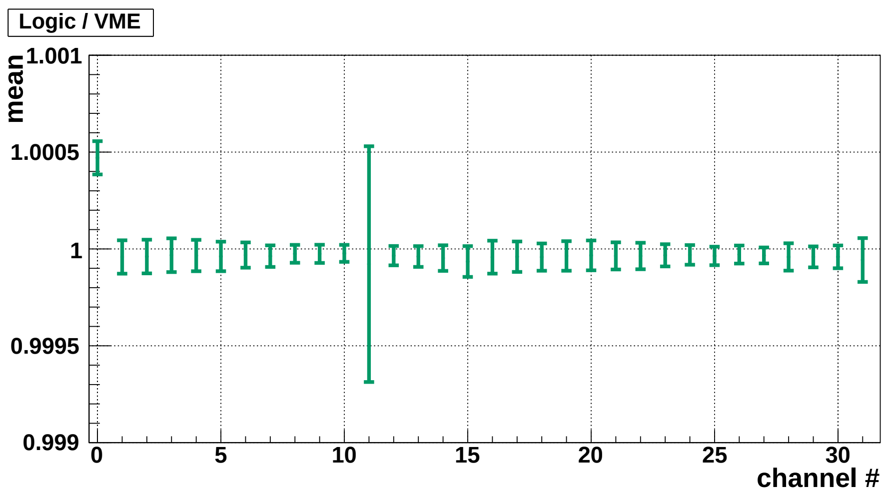

Figure 7.9: *Averaged ratios of all channels, measured with the scalers Logic and VME.*

Comparison between Logic and Scaler scalers

Due to the fact, that the implemented scalers in the FPGA (Logic) work properly, the ratios between the Logic and the Scaler counter represent direct comparisons of the old and the new electronics. Figure 7.10 depicts the rates and the ratios of the two scalers for channel 01. The mean value $\overline{r} = 0.9992 \pm 0.0001$ is 0.8‰ lower than the expected ratio of 1. The difference to 1 amounts to $8\,\sigma$. The mean of the pull distribution is compatible with 0. The width is greater than 1 which evidences a higher fluctuation of the ratios around the average. This could be induced by the timing of the readout.

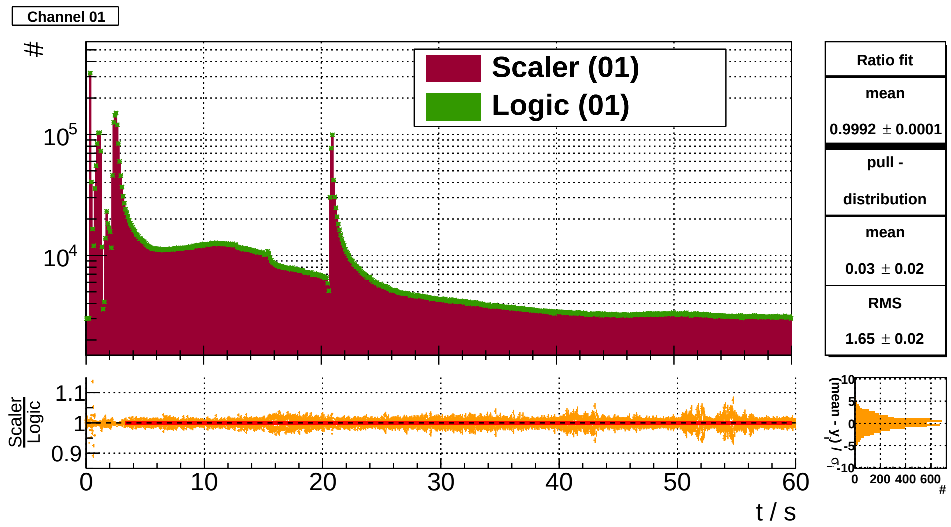

Figure 7.10: *Ratio over time for the scalers Logic and Scaler of channel 01.*

Figure 7.11 shows the ratios derived from the scalers Scaler and Logic for all channels. The ratios for the channels 02 up to 30 are at the same order as the one for channel 01. The ratio for channel 31 is around 0.94 what is obviously far away from all of the other channels. A deeper investigation depicts that this deviation originates in a software bug of the old electronics: channel 31 of the data stream was wrongly filled with the data of channel 00. Therefore all measurements with channel 31 of the old electronics have this artefact. The deviation of channel 00 is unknown and cannot be explained.

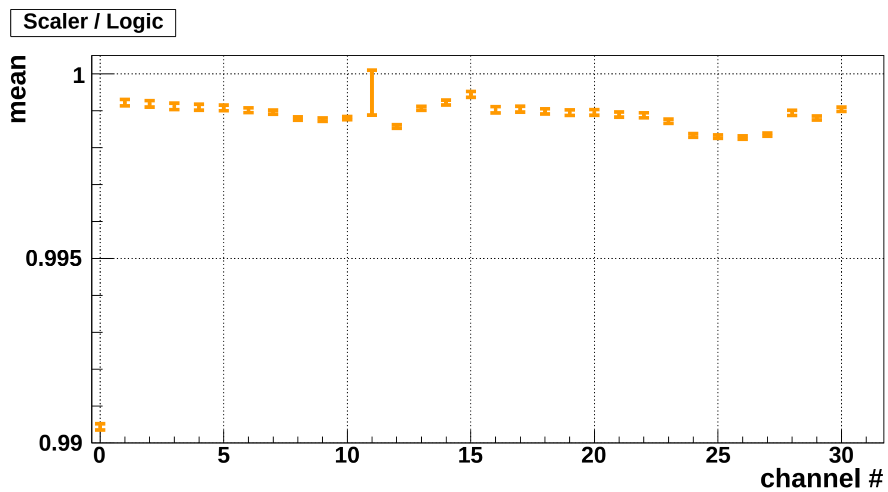

Figure 7.11: *Averaged ratios between the scalers Logic and Scaler for all channels.*

Comparison between VME and Scaler scalers

Considering that the scalers Logic and VME are counting the same rates, the ratio between the scalers Scaler and VME should be the same as the ratio between the scalers Scaler and Logic. The ratio between the scalers VME and Scaler (figure 7.12) shows the same artefacts as the one between the scalers Scaler and Logic. Only the pull distribution is wider ($RMS = 1.32$), what may be caused due to different readout times of the electronic systems. The averaged ratios between the scalers

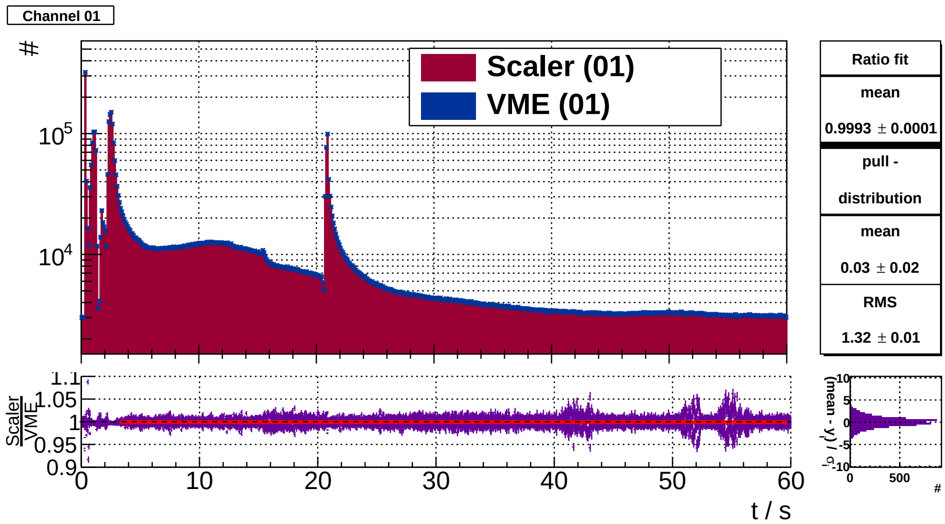

Figure 7.12: *Ratio over time between the scales Scaler and VME of channel* 01.

VME and Scaler of all channels are plotted in figure 7.13. The pattern is the same as the one for the ratios Scaler/Logic (figure 7.11), including the same artefacts of channel 00 and 31. The higher rate of the new electronics could be caused by

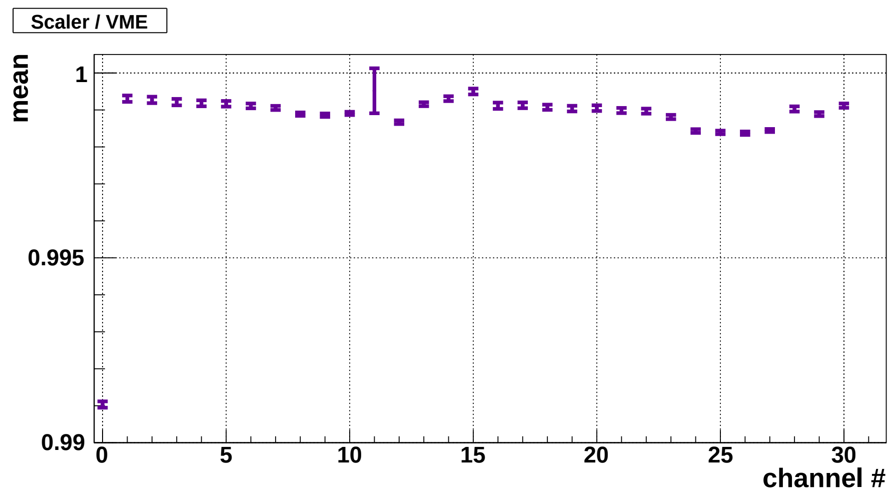

Figure 7.13: *Averaged ratios between the scalers VME and Scaler for all channels.*

different sensitivities of the new and old electronics concerning to the logic levels of the signals. Additionally the dead time of the new system could be lesser than the one of the old system. This would cause to higher rates in the new electronics, as measured. The higher rate effect can be ignored if both systems measure the same asymmetry for each ring. Section 7.2.6 discusses the analysis of the asymmetries.

Pull distributions

The mean and the RMS of all pull distributions are depicted in figure 7.14. The x-axis represents the channel number of each scaler (channels $00-15$: semiring left $14-29$, channels $16-31$: semiring right $14-29$). The y value of each point relates to the mean value of the pull distribution. The RMS values are indicated by the error bar. The azure graph corresponds to the comparison of the two new scalers. All mean

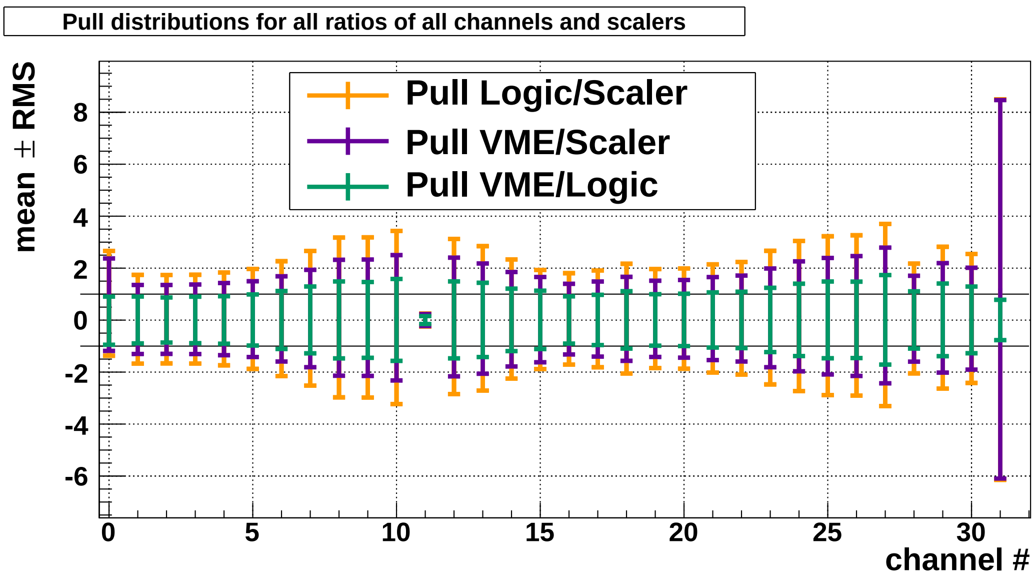

Figure 7.14: *Pull distributions for all ratios of scalers for all channels.*

values are compatible with zero and the RMS fluctuate around 1. Channel 11 which measured only noise has to be ignored. The other two graphs show the comparison of the new and the old electronics. Neglecting the channels 00, 11 and 31 the mean values are compatible with zero. The RMS values of all channels are larger than 1 which may correspond to the timing effect during the readout of the new and the old electronics.

7.2.6 Measured asymmetries with all scalers

The next step, in verifying the correct function of the new electronics, is to compare the asymmetries measured with all three scalers for each semiring pair.

Assuming N_{L} and N_{R} as the rates in the left and right semirings, the asymmetry $A_{\text{L-R}}$ is defined by:

$$A_{\text{L-R}} = \frac{N_{\mathrm{L}} - N_{\mathrm{R}}}{N_{\mathrm{L}} + N_{\mathrm{R}}}. \tag{7.7}$$

The errors for the counted rates are given by:

$$\sigma_{N_{\mathrm{L}}} = \sqrt{N_{\mathrm{L}}} \text{ and } \sigma_{N_{\mathrm{R}}} = \sqrt{N_{\mathrm{R}}}. \tag{7.8}$$

Assuming, that the rates in the left and right semirings (N_{L}, N_{R}) are uncorrelated, the associated error propagation is developed in the formulas 7.9 to 7.12:

$$\sigma^2_{A_{\text{L-R}}} = \left(\frac{\mathrm{d}A_{\text{L-R}}}{\mathrm{d}N_{\mathrm{L}}} \cdot \sigma_{N_{\mathrm{L}}}\right)^2 + \left(\frac{\mathrm{d}A_{\text{L-R}}}{\mathrm{d}N_{\mathrm{R}}} \cdot \sigma_{N_{\mathrm{R}}}\right)^2 + 2\frac{\mathrm{d}A_{\text{L-R}}}{\mathrm{d}N_{\mathrm{L}}}\frac{\mathrm{d}A_{\text{L-R}}}{\mathrm{d}N_{\mathrm{R}}} \cdot \underbrace{\mathrm{cov}\left(N_{\mathrm{L}}, N_{\mathrm{R}}\right)}_{=0} \tag{7.9}$$

$$= \left(\frac{2N_{\mathrm{R}}}{(N_{\mathrm{L}} + N_{\mathrm{R}})^2} \cdot \sigma_{N_{\mathrm{L}}}\right)^2 + \left(\frac{2N_{\mathrm{L}}}{(N_{\mathrm{L}} + N_{\mathrm{R}})^2} \cdot \sigma_{N_{\mathrm{R}}}\right)^2 \tag{7.10}$$

$$= \frac{4 \cdot N_{\mathrm{L}} N_{\mathrm{R}}^2}{(N_{\mathrm{L}} + N_{\mathrm{R}})^4} + \frac{4 \cdot N_{\mathrm{L}}^2 N_{\mathrm{R}}}{(N_{\mathrm{L}} + N_{\mathrm{R}})^4} \tag{7.11}$$

$$= \frac{4 \cdot N_{\mathrm{L}} N_{\mathrm{R}}}{(N_{\mathrm{L}} + N_{\mathrm{R}})^3}. \tag{7.12}$$

Averaging the asymmetries over time results in the plots shown in figure 7.15.

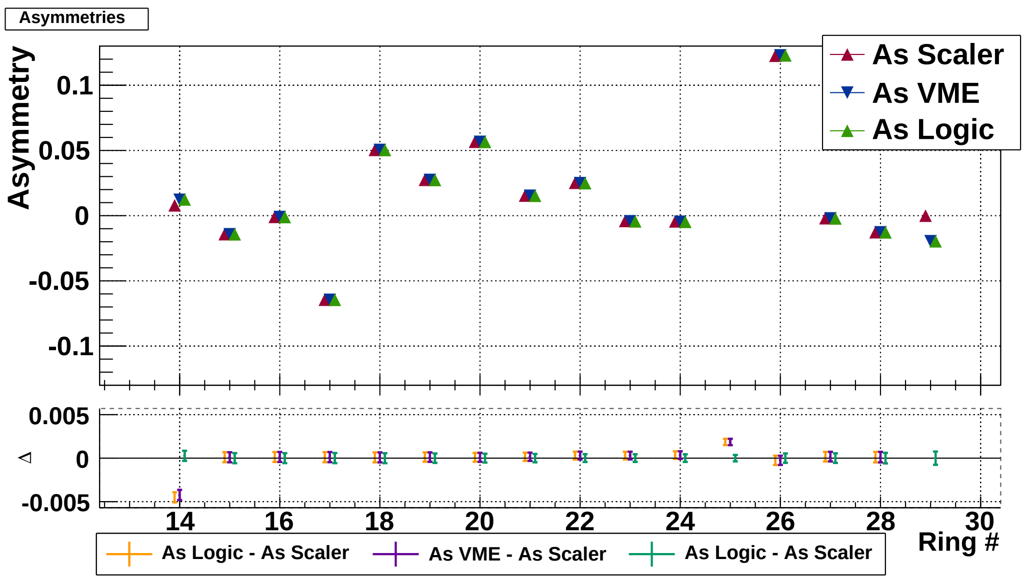

Figure 7.15: *Asymmetries for the rings* 14 *to* 29*, measured by all three scalers. The bottom graph contains the differences between the asymmetries per ring.*

The upper plot contains the Left-Right asymmetries for all rings, measured by all scalers. The asymmetry of unpolaraised protons should be zero. Different detection efficiencies of opposite semirings lead to non-vanishing asymmetries which are measured by the scalers. Each of the three points per ring indicates the asymmetry measured by one of the three scalers. Correct scalers and electronics result in three points lying on one horizontal line per ring.

The difference between the asymmetries per ring is plotted in the bottom. Except the rings 14, 25 and 29 the differences of the asymmetries are all compatible with zero. The non-vanishing difference in the asymmetries of rings 25 and 29 can be explained by the non-functional channels 11 and 31. The difference of the asymmetry between the old and the new electronics for ring 14 is around $5\,\sigma$ below zero. This corresponds to the lower ratio of channel 00 between the old and the new electronics. Since the two scalers of the new electronics measure the same asymmetry, the measurement of the old electronics could be incorrect for this ring.

7.2.7 Summary

The installation and implementation of the V1495 board and the SIS3820 module in the existing framework proceeded successfully. Except the mentioned problems with channel 11 and 31, the comparison of the measurements with the two systems shows consistent asymmetries. Altogether, the new system is successfully installed and can replace the existing modules.

8 Beamtime September 2013

This chapter deals with a measurement of polarised deuteron beams with a momentum of $p = 970\,\mathrm{MeV/c}$, during the September beamtime[15]. The first section summarises the equations to describe the used spin manipulations in COSY. Section 8.3 contains a beam polarisation measurement during a Froissart Stora Scan. The development of the beam polarisation, induced by a resonant excitation by the RF solenoid is shown in the last part of this chapter.

8.1 Spin motion in storage rings

The particle's spin precession is described in the rest frame of the particle by

$$\frac{\mathrm{d}\vec{S}^*}{\mathrm{d}t} = \vec{\mu} \times \vec{B}^*, \tag{8.1}$$

where $\vec{S}^*$ is the spin vector, μ is the magnetic moment of the particle and $\vec{B}^*$ is the magnetic field. Transforming in the lab frame yields the Thomas Bargmann Michel Telegdi (Thomas-BMT) equation [2, 11]

$$\begin{aligned} \frac{\mathrm{d}\vec{S}}{\mathrm{d}t} &= \vec{S} \times \vec{\Omega} \quad \text{with} \\ \vec{\Omega} &= \frac{q}{m\gamma}\left((1+\gamma G)\,\vec{B}_\perp + (1+G)\,\vec{B}_\parallel - \left(\gamma G + \frac{\gamma}{1+\gamma}\right)\frac{\vec{\beta}\times\vec{E}}{c}\right), \end{aligned} \tag{8.2}$$

where $\vec{B}_\perp$ and $\vec{B}_\parallel$ points perpendicular respectively parallel to the particle motion $\vec{\beta}$. G is the anomalous magnetic moment of the particle and γ is the usual Lorentz factor. For the special case of a pure magnetic ring with $\vec{B}_\parallel = \vec{0}$, the Thomas-BMT equation simplifies to

$$\frac{\mathrm{d}\vec{S}}{\mathrm{d}t} = \frac{q}{m\gamma}\,(1+\gamma G)\,\vec{S} \times \vec{B}_\perp. \tag{8.3}$$

The spin tune ν_s is the number of spin turns per particle turn with respect to the particle's momentum

$$\nu_s = \gamma \cdot G. \tag{8.4}$$

[15]September beamtime: 9th of September to 22th of September 2013

The selected momentum of $p = 970\,\mathrm{MeV/c}$ corresponds to $\gamma = 1.126$. The anomalous magnetic moment for a deuteron is $G = -0.1429$. These two values yield to

$$\nu_s = -0.16098. \tag{8.5}$$

According to equation 8.2, a radio frequency magnetic field parallel to the direction of motion induces a spin rotation. If the frequency of this field fulfil the resonance equation

$$f_{\mathrm{R}} = f_0\,(k \pm \nu_s)\,, k \in \mathbb{N}, \tag{8.6}$$

the polarisation vector of the beam changes the direction [11, p. 50]. The orbital frequency f_0 of a deuteron beam with $p = 970\,\mathrm{MeV/c}$ is $f_0 = 750.2\,\mathrm{kHz}$ in COSY.

The RF solenoid, shown in figure 8.1, generates the radio frequency, spin manipulating, magnetic field in COSY. The frequency and the strength of the applied magnetic field influence the development of the vertical beam polarisation. Sections 8.3 and 8.4 present measurements with different settings of the frequency and the amplitude of the RF solenoid.

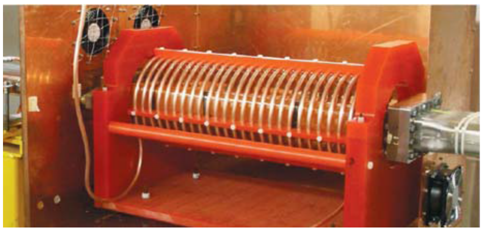

Figure 8.1: *RF solenoid for spin manipulations. [11, p. 92]*

8.2 Spin coherence time

Due to the Thomas-BMT equation the spins of all particles precess with the angle momentum $\vec{\Omega}$ which depends on the particle's Lorentz factor γ. A momentum spread of the particles in the accelerator leads to different Lorentz factors of the particles which leads to different spin tunes of the particles. Whilst the beam polarisation is vertical, these spin tune spread does not influence the measured polarisation because the detector measures the projection of the spins to the vertical axis (see figure 8.2).

But for a horizontally polarised beam, the spin tune spread influences the polarisation. At the injection of the particles all spins are pointing in one direction, but after a certain time the spins precess with different velocities around the so called spin closed-orbit (green vector). Due to this precession, the horizontal polarisation of the beam vanishes. A characterising time for the polarisation drop is the spin coherence time (SCT). Figure 8.3 illustrates the described effect.

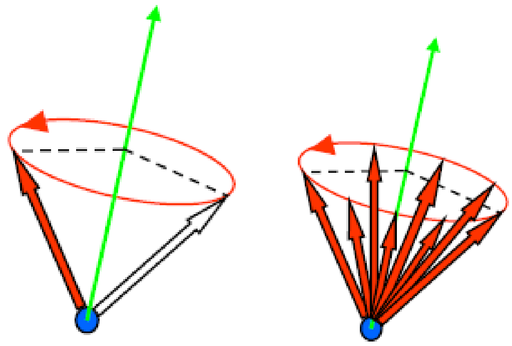

(a) *All spins are oriented in one direction.*

(b) *After a certain time the spins are aligned on a cone.*

Figure 8.2: *Spin time evolution of a vertical polarised beam. [18, p. 19]*

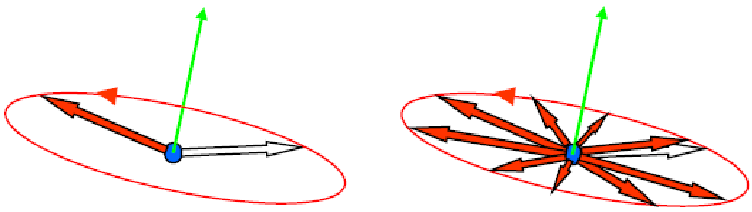

(a) *All spins are oriented in one direction.*

(b) *After a certain time the spins decohere and the polarisation vanishes.*

Figure 8.3: *Spin time evolution of a horizontal polarised beam. [18, p. 19]*

8.3 Froissart Stora Scan

By passing a spin tune resonance (equation 8.6), the change in polarisation is described by the Froissart Stora equation [11, p. 51]

$$\frac{P_v^f}{P_v^i} = 2\exp\left(\frac{-(\pi\epsilon_r f_{\mathrm{R}})^2}{\Delta f/\Delta t}\right) - 1, \tag{8.7}$$

where $\Delta f/\Delta t$ is the frequency shift speed of the RF solenoid, f_{R} is the crossed resonance frequency and ϵ_r is the resonance strength. The initial vector polarisation is P_v^i and the final one after the crossing is P_v^f. An example of resonance crossing for the settings

$$\Delta f = 40\,\text{Hz} \tag{8.8}$$

$$\Delta t = 40\,\text{s} \tag{8.9}$$

is shown in figure 8.4. The spin state 01 corresponds to a vertical upwards pointing

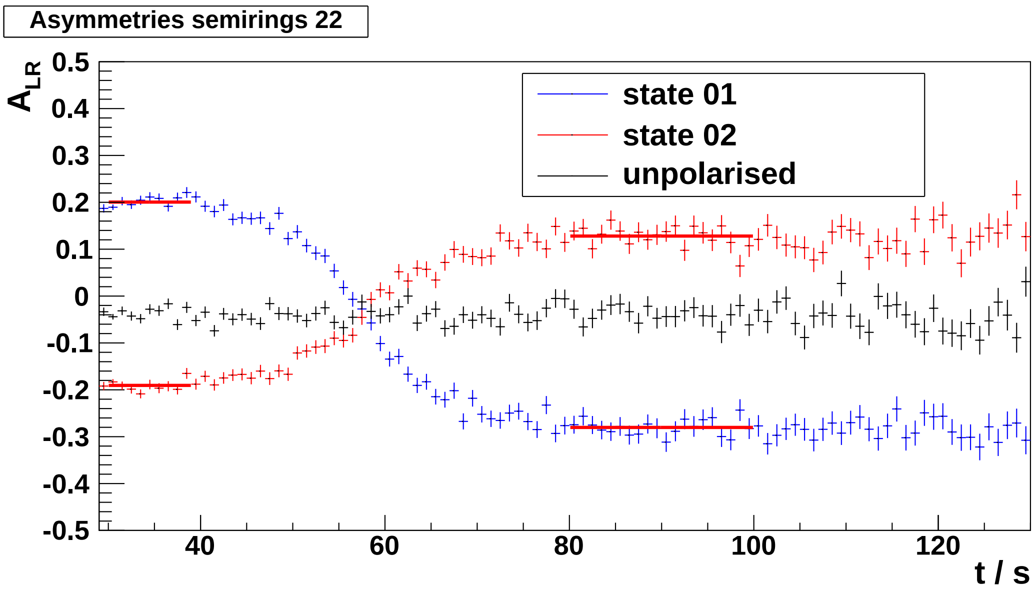

Figure 8.4: *Measurement of the Left-Right asymmetry with the semirings 22 during the Froissart Stora Scan.*

polarisation of the injected beam (blue data points). State 02 is a vertical downwards pointing polarisation at the injection (red data points). The black data points correspond to an unpolarised beam and represent the detector efficiency asymmetries. The data points shown are the asymmetries measured by the semiring pair 22. All of the other semiring pairs measure asymmetry changes with different amplitudes as the analysing power depends on solid angle, covered by the semirings.

The asymmetries before the resonance crossing and after the resonance crossing are determined by fitting a straight line for the two time ranges $30\,\text{s} - 39\,\text{s}$ and $80\,\text{s} - 100\,\text{s}$. These two lines are fitted on the data for state 01 and state 02. The difference between the resulting asymmetries $A_{\text{LR,max}}$ and $A_{\text{LR,min}}$ is proportional to the analysing power in the angle range of the semiring pair. These differences are plotted in figure 8.5 versus the semiring pairs $14 - 29$. The data point corresponding to the semiring pair 25 is not printed, because the rates of semiring left 25 are zero. The highest difference exists for the semiring pairs $22, 23, 24$ and 26. In the next section these semirings are used to measure the time development of the polarisation by a resonance excitation due to the RF solenoid.

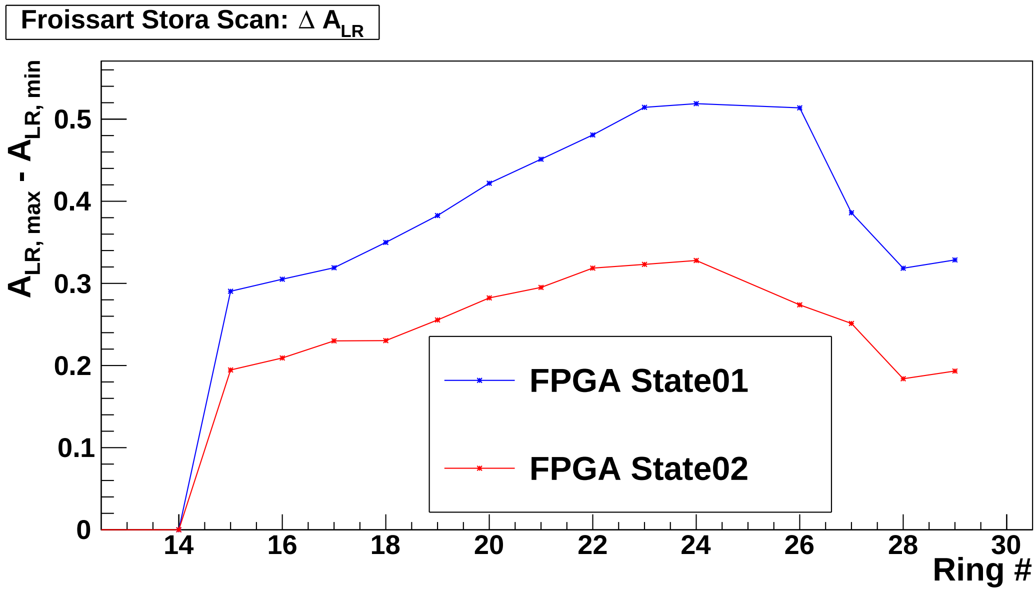

Figure 8.5: *Difference of the Asymmetries before and after the induced spin flip measured by all semiring pairs.*

8.4 Resonant excitation

A resonant excitation of the spins induces a rotation of the spin vectors. This rotations lead to an oscillation of the measured Left-Right asymmetries in the EDDA detector. By crossing the horizontal plane, the spin vectors of all particles distribute in the horizontal plane, which leads to a decoherence of the polarisation. This decoherence effect is in first order expressed by an exponential damping of the oscillation.

Calculating the cross ratio is a method to analyse the data with respect to both spin states. The cross ratio CR is given by

$$CR_{\mathrm{LR}} = \frac{\sqrt{L^{\uparrow} \cdot R^{\downarrow}} - \sqrt{L^{\downarrow} \cdot R^{\uparrow}}}{\sqrt{L^{\uparrow} \cdot R^{\downarrow}} + \sqrt{L^{\downarrow} \cdot R^{\uparrow}}}, \tag{8.10}$$

where $L^{\uparrow}$ and $L^{\downarrow}$ are the counted rates in the Left category for spin state 01 respectively spin state 02. The counted rates in the Right category for both spin states are represented by $R^{\uparrow}$ and $R^{\downarrow}$. The figures 8.6 to 8.8 show the resulting oscillations for different settings of the RF solenoid. The polarisation of the beam results in a cross ratio about 0.18 at the beginning of the cycle. The RF solenoid is switched on 39 s after the cycle started.

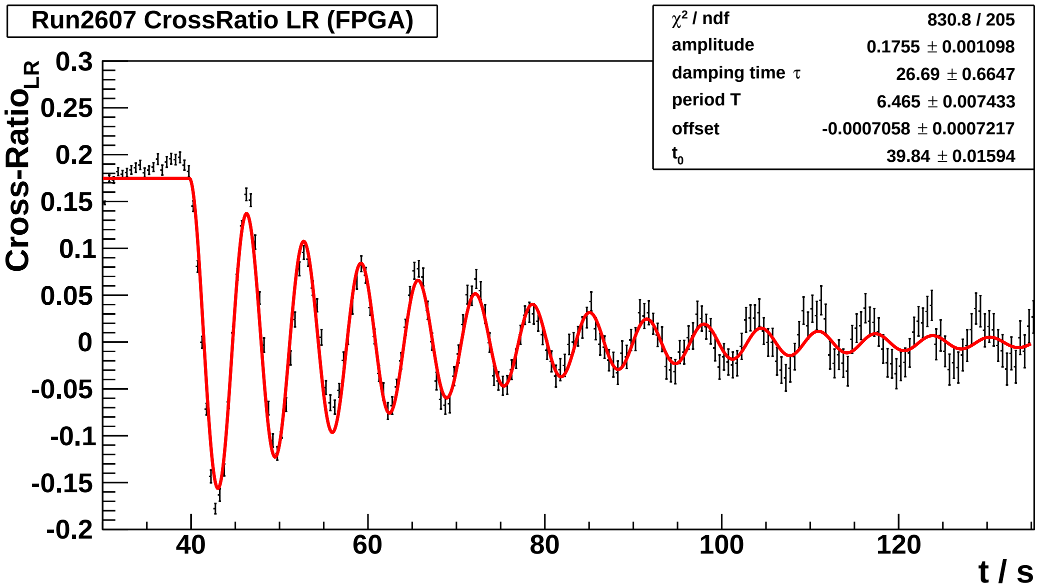

Figure 8.6: *RF solenoid settings: frequency:* 871432.1 *Hz, amplitude:* 1.5*.*

The measured cross ratio is described by the mentioned damped oscillation. The fitted functions are given by

$$CR\,(t) = \begin{cases} A + offset & t < t_0 \\ A \cdot e^{(-t+t_0))/\tau} \cdot \cos(2\pi \cdot t/T) + offset & t \geq t_0 \end{cases} \tag{8.11}$$

All shown plots are examples of a systematic analysis of the spin development for different RF solenoid settings[16]. The plots present the polarisation development, measured by the new electronic system and are not explained in more details. All plots demonstrate that the new system works properly and measures the evolution of the beam polarisation during a resonance excitation of the particles' spins.

[16] A detailed analysis of the data and a comparison with a simulation is in preparation by Marcel Rosenthal.

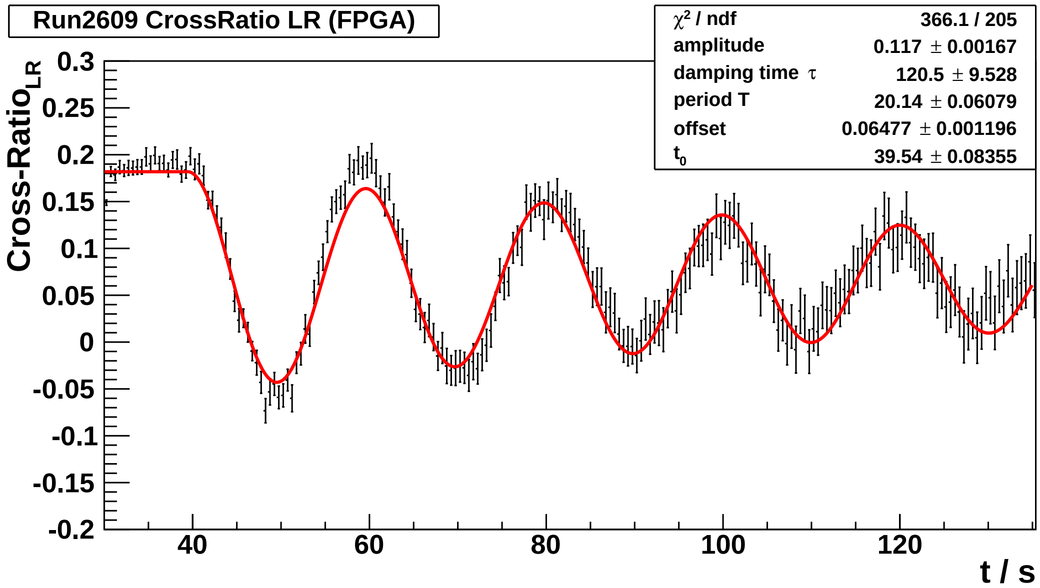

Figure 8.7: *RF solenoid settings: frequency:* 871432.1 *Hz, amplitude:* 0.05.

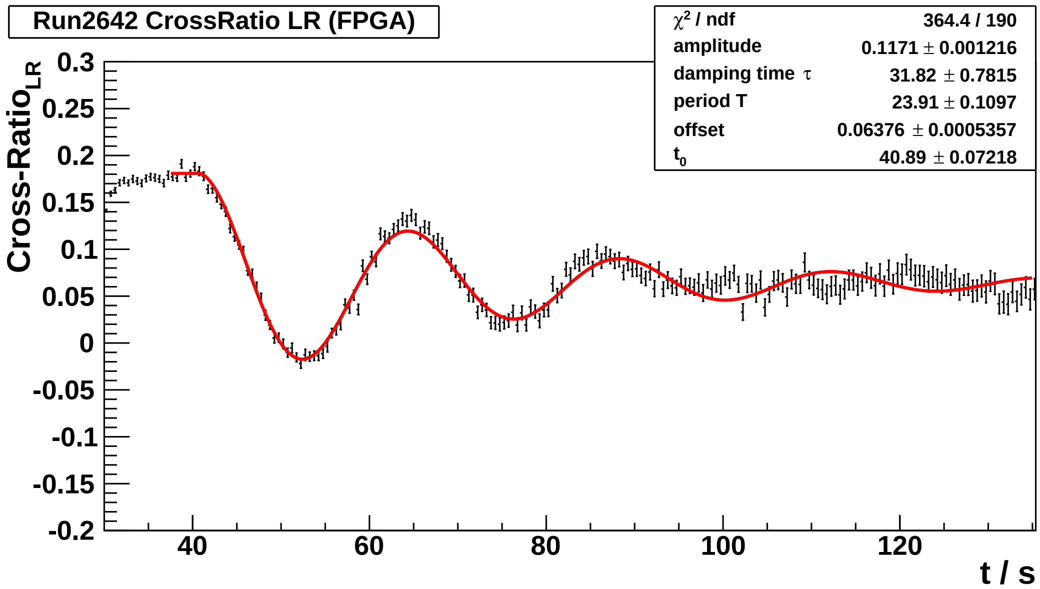

Figure 8.8: *RF solenoid settings: frequency:* 1622036.17 *Hz, amplitude:* 0.05.

9 Conclusion & Outlook

Conclusion

In this master thesis the development and installation of a new readout electronic scheme for the EDDA detector at COSY is presented.

The developed firmware runs successfully on the onboard FPGA of the general purpose VME board. The firmware implements a signal processing chain which sifts out the elastic scattered particles and counts the detected rates in different solid angles. Combining the rates in different solid angles makes a polarisation measurement of the circulating beam in COSY possible.

The upgraded readout electronics undertakes the functions of the existing programmable logic units. In addition, the new system combines the signals of the semirings and the bars of the EDDA detector which allows a measurement of the Up-Down asymmetry apart from the Left-Right asymmetry.

To handle the data, they are added to the existing data stream and are included in the EDDA DAQ system. The data, taken in the July beamtime, show a correct cabling of the module and a right data transfer to the DAQ computer.

In the September beamtime, the upgraded readout system measured the polarisation evolution of a deuteron beam. To these belong a recorded polarisation flip, induced by a Froissart Stora scan. Apart from the Froissart Stora scan a monitoring of an oscillation of the beam polarisation, induced by an on resonance running RF solenoid, was demonstrated successfully.

The installed system is ready to use and features beam polarisation studies by the JEDI collaboration.

Outlook

The current configuration of the V1495 board has twelve free input ports and 60 free output ports. The output ports can be used to tag the Up, Right, Left and Down events for each θ range with a time stamp by the external TDC module. This configuration could be used for detailed lifetime studies of the beam polarisation.

An idea for the use of the free incoming ports is a new time stamping system for the DAQ. Presently the time stamps of the DAQ depend on the timing system of COSY, which leads to a start of the timing system with every new cycle. For detailed measurements over many cycles, an independent timing system is necessary. The implementation of a clock in the FPGA which runs independently from the COSY time stamping system and starts with every run is a possible solution for the needed timing system. The maximum frequency of this clock is 400 MHz for the usage of an internal clock or 250 MHz for the usage of an external clock. The external frequency is limited by the bandwidth of the incoming ports. These frequencies lead to a maximum resolution of 2.5 ns respectively 4 ns.

Currently, the memory usage of the FPGA is only 1%, so the programming of additional masks for finer energy ranges is possible. This should lead to triggers with a higher purity. Free resources of the FPGA (74% of the LEs are available) can be used for the implementation of other features, needed for detailed studies by the JEDI collaboration.

An additional improvement might be the implementation of a VME block transfer mode, which allows faster reading and writing processes to the module.

For an absolute polarisation measurement of a deuteron beam, an estimation of effective analysing powers for the detected events is necessary.

Bibliography

[1] Altera, San Jose, CA 95134. *Cyclone Device Handbook, Volume 1*, May 2008.

[2] V. Bargmann, Louis Michel, and V. L. Telegdi. Precession of the Polarization of Particles Moving in a Homogeneous Electromagnetic Field. *Phys. Rev. Lett.*, 2:435–436, May 1959.

[3] C.L. Bennett et al. First year Wilkinson Microwave Anisotropy Probe (WMAP) observations: Preliminary maps and basic results. *Astrophys.J.Suppl.*, 148:1, 2003.

[4] Karsten Büßer. *Anregungsfunktionen und Winkelverteilungen der Analysierstärke der elastischen Proton-Proton-Streuung bei mittleren Energien.* PhD thesis, Universität Hamburg, 1999.

[5] CAEN Electronic Instrumentation, Viareggio, Italy. *Technical Information Manual DEMO1 GATE PATTERN*, revision n. 1 edition, June 2010.

[6] CAEN Electronic Instrumentation, Viareggio, Italy. *Technical Information Manual MOD. V1495 GENERAL PURPOSE VME BOARD*, revision n. 13 edition, July 2012.

[7] CAEN Electronic Instrumentation. V1495 General Purpose VME Board. `http://www.caen.it/csite/CaenProd.jsp?parent=11&idmod=705`, (accessed: 22/09/2013), September 2013.

[8] EDDA Collaboration. EDDA Plots und Bilder. `http://edda.hiskp.uni-bonn.de/protected/bilder/topDoNotEdit.html`, (accessed: 17/09/2013), September 2013.

[9] D. Fick. *Einführung in die Kernphysik mit polarisierten Teilchen.* Bibliographisches Institut Mannheim/Wien/Zürich, 1971.

[10] Takeshi Fukuyama. Searching for New Physics beyond the Standard Model in Electric Dipole Moment. *Int.J.Mod.Phys.*, A27:1230015, 2012.

[11] Andreas Lehrach. *Strahl- und Spindynamik von Hadronenstrahlen in Mittelenergie-Ringbeschleunigern.* Forschungszentrum Jülich, 2008.

[12] Bernd Lorentz. Private communication.

[13] R. Maier. Cooler synchrotron {COSY} — Performance and perspectives . *Nuclear Instruments and Methods in Physics Research Section A: Accelerators, Spectrometers, Detectors and Associated Equipment*, 390(1–2):1 – 8, 1997.

[14] Gerald G Ohlsen. Polarization transfer and spin correlation experiments in nuclear physics. *Reports on Progress in Physics*, 35(2):717, 1972.

[15] W. Pauli. Zur Quantenmechanik des magnetischen Elektrons. *Zeitschrift für Physik*, 43(9-10):601–623, 1927.

[16] J.M. Pendlebury and E.A. Hinds. Particle electric dipole moments. *Nuclear Instruments and Methods in Physics Research Section A: Accelerators, Spectrometers, Detectors and Associated Equipment*, 440(3):471 – 478, 2000.

[17] Jörg Pretz. Measurement of Permanent Electric Dipole Moments of Charged Hadrons in Storage Rings. *Hyperfine Interact.*, 214(1-3):111–117, 2013.

[18] Jörg Pretz et. al. Search for Permanent Electric Dipole Moments at COSY - Step 1: Spin coherence and systematic error studies, May 2013.

[19] Andrei D Sakharov. Violation of CP in variance, C asymmetry, and baryon asymmetry of the universe. *Soviet Physics Uspekhi*, 34(5):392, 1991.

[20] Edward J. Stephenson. Electronics and Data Acquisition Requirements R&D for Deuteron Electric Dipole Moment Search Study of Longitudinal Polarization Lifetime.

[21] E. Weise. EDDA Internal Report 00-01, 2000.

[22] Knut Woller. *Die Außenschale des EDDA-Detektors an COSY und erste Ergebnisse zur elastischen Proton-Proton-Streuung bei T=1505 MeV und T=2201 MeV*. PhD thesis, Universität Hamburg, 1996.

List of Figures

List of Tables

List of Listings

A Appendix

A.1 Kinematics of the elastic pp scattering

Looking at the scattering of a particle with mass m_{B} and momentum p_{B} and a in the lab system resting target with mass m_{T}. The elastic scattered particles are labelled 1 and 2. Without loss of generality the momentum of the beam particle points in z-direction. The four-momentums of the particles in the lab frame are:

$$\boldsymbol{P}_{\mathrm{B}} = \begin{pmatrix} E_{\mathrm{B}} \\ 0 \\ 0 \\ p_{\mathrm{B}} \end{pmatrix} \boldsymbol{P}_{\mathrm{T}} = \begin{pmatrix} m_{\mathrm{T}} \\ 0 \\ 0 \\ 0 \end{pmatrix} \boldsymbol{P_1} = \begin{pmatrix} E_1 \\ \\ \vec{p}_1 \\ \\ \end{pmatrix} \boldsymbol{P_2} = \begin{pmatrix} E_2 \\ \\ \vec{p}_2 \\ \\ \end{pmatrix}. \tag{A.1}$$

The following relations apply to the center of mass system (CMS):

$$\boldsymbol{P}_{\mathrm{B}}{}' = \begin{pmatrix} E'_{\mathrm{B}} \\ 0 \\ 0 \\ p'_{\mathrm{B}} \end{pmatrix} \boldsymbol{P}_{\mathrm{T}}{}' = \begin{pmatrix} E'_{\mathrm{T}} \\ 0 \\ 0 \\ p'_{\mathrm{T}} \end{pmatrix} \boldsymbol{P_1}{}' = \begin{pmatrix} E'_1 \\ \\ \vec{p}'_1 \\ \\ \end{pmatrix} \boldsymbol{P_2}{}' = \begin{pmatrix} E'_2 \\ \\ \vec{p}'_2 \\ \\ \end{pmatrix}. \tag{A.2}$$

The transformation between the center of mass system and the lab frame is described by the Lorentz transformation:

$$\begin{pmatrix} E \\ p_x \\ p_y \\ p_z \end{pmatrix} = \begin{pmatrix} \gamma & 0 & 0 & \gamma\beta \\ 0 & 1 & 0 & 0 \\ 0 & 0 & 1 & 0 \\ \gamma\beta & 0 & 0 & \gamma \end{pmatrix} \cdot \begin{pmatrix} E' \\ p'_x \\ p'_y \\ p'_z \end{pmatrix}. \tag{A.3}$$

The variables β and γ are defined by the following equation:

$$\beta = \frac{v_{\mathrm{B}}}{c} = \frac{p_{\mathrm{B}}}{E_{\mathrm{B}}} \text{ and } \gamma = \frac{1}{\sqrt{1-\beta^2}}. \tag{A.4}$$

The momenta and the scattering angle are shown in figure A.1.

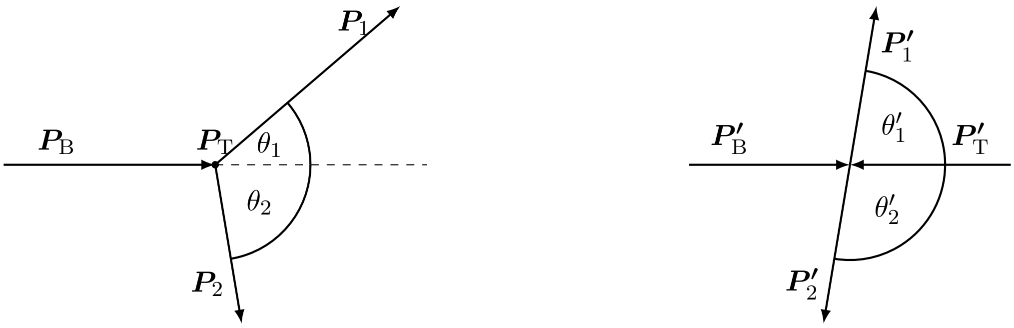

Figure A.1: *Momenta and angles in the rest frame and the CMS system.*

In the CMS system the particle momenta are:

$$\begin{aligned} \vec{p}'_\mathrm{B} + \vec{p}'_\mathrm{T} = \vec{0} &\Leftrightarrow \vec{p}'_\mathrm{B} = -\vec{p}'_\mathrm{T} \\ \vec{p}'_1 + \vec{p}'_2 = \vec{0} &\Leftrightarrow \vec{p}'_1 \ = -\vec{p}'_2 \end{aligned}. \tag{A.5}$$

The Lorentz-invariant

$$\boldsymbol{p}^2 = E^2 - \vec{p}^2 = m^2 \tag{A.6}$$

contains the relation between energy, momentum and mass of a particle. The Mandelstam variable s leads to:

$$\begin{aligned} s &= (\boldsymbol{p'_1} + \boldsymbol{p'_2})^2 \\ &= \boldsymbol{p'_1}^2 + \boldsymbol{p'_2}^2 + 2\,\boldsymbol{p'_1}\,\boldsymbol{p'_2} \\ &= m_1^2 + m_2^2 + 2 \cdot (E'_1 E'_2 - \vec{p}'_1 \cdot \vec{p}'_2)\,. \end{aligned} \tag{A.7}$$

The relation between the energies results from:

$$s = \begin{pmatrix} E'_1 + E'_2 \\ \vec{p}'_1 + \vec{p}'_2 \end{pmatrix}^2 \overset{(\vec{p}_{1'} + \vec{p}_{2'} = \vec{0})}{=} (E'_1 + E'_2)^2\,. \tag{A.8}$$

Solving to E'_1 results in:

$$E'_1 = \sqrt{s} - E'_2. \tag{A.9}$$

Combining equation (A.9), formula (A.7) and the equation $\vec{p}'_1 = -\vec{p}'_2$ yields:

$$\begin{aligned} s &= m_1^2 + m_2^2 + 2\,\vec{p}'^2_1 + 2E'_1\left(\sqrt{s} - E'_1\right) \\ &= m_1^2 + m_2^2 - 2\underbrace{\left(E'^2_1 - \vec{p}'^2_1\right)}_{m_1^2} + 2E'_1\sqrt{s} \\ &= m_2^2 - m_1^2 + 2E'_1\sqrt{s}. \end{aligned} \tag{A.10}$$

Solving for the energy E_1' and a similar estimation of energy E_2' leads to:

$$\begin{aligned} E_1' &= \frac{s + m_1^2 - m_2^2}{2\sqrt{s}} \\ E_2' &= \frac{s + m_2^2 - m_1^2}{2\sqrt{s}}. \end{aligned} \tag{A.11}$$

The scattering angles θ_1 and θ_2 are measurable in the lab system. These angles are defined by:

$$\sin(\theta_1) = \frac{|\vec{p}_{1,\mathrm{xy}}|}{|\vec{p}_1|} = \frac{\sqrt{p_{1,\mathrm{x}}^2 + p_{1,\mathrm{y}}^2}}{p_1} = \frac{p_{1,\mathrm{xy}}}{p_1} \tag{A.12}$$

$$\cos(\theta_1) = \frac{|\vec{p}_{1,\mathrm{z}}|}{|\vec{p}_1|} = \frac{p_{1,\mathrm{z}}}{p_1}. \tag{A.13}$$

The variable $\tan(\theta)$ is given by:

$$\tan(\theta_1) = \frac{\sin(\theta_1)}{\cos(\theta_1)} = \frac{p_{1,\mathrm{xy}}}{p_{1,\mathrm{z}}}. \tag{A.14}$$

Transforming to the CMS system results in:

$$\tan(\theta_1) = \frac{p'_{1,\mathrm{xy}}}{\gamma\left(p'_{1,\mathrm{z}} + \beta_1 E_1'\right)}. \tag{A.15}$$

With the equations:

$$\beta_1' = \frac{p_1'}{E_1'} \tag{A.16}$$

$$\sin(\theta_1') = \frac{p'_{1,\mathrm{xy}}}{p_1'} \tag{A.17}$$

$$\cos(\theta_1') = \frac{p'_{1,\mathrm{z}}}{p_1'} \tag{A.18}$$

the angle θ_1 is defined by:

$$\tan(\theta_1) = \frac{\sin(\theta_1')}{\gamma\left(\cos(\theta_1') + \frac{\beta}{\beta_1'}\right)}. \tag{A.19}$$

The analogue equation for $\tan(\theta_2)$ is defined in a similar way. Considering the condition $\theta_1' + \theta_2' = \pi$ in the center of mass system results in:

$$\sin(\theta_2') = \sin(\theta_1') \text{ und } \cos(\theta_2') = -\cos(\theta_1'). \tag{A.20}$$

The factors β_1', β_2' and β are calculated by the following relations.

$$\beta = \frac{|\vec{p}_\mathrm{B} + \vec{p}_\mathrm{T}|}{E_\mathrm{B} + E_\mathrm{T}} \overset{(\vec{p}_\mathrm{T}=\vec{0})}{=} \frac{p_\mathrm{B}}{E_\mathrm{B} + E_\mathrm{T}} = \frac{\sqrt{E_\mathrm{B}^2 - m_\mathrm{B}^2}}{E_\mathrm{B} + E_\mathrm{T}} \tag{A.21}$$

$$\beta_1 = \frac{p_1'}{E_1'} = \frac{\sqrt{E_1'^2 - m_1^2}}{E_1'} \tag{A.22}$$

$$\beta_2 = \frac{p_2'}{E_2'} = \frac{\sqrt{E_2'^2 - m_2^2}}{E_2'}. \tag{A.23}$$

The elastic proton-proton scattering is discussed in the following. The masses and the energy of the target particle simplify to:

$$m_\mathrm{B} = m_\mathrm{T} = E_\mathrm{T} = m_1 = m_2 = m_\mathrm{P}. \tag{A.24}$$

Equation (A.11) simplifies to:

$$E_1' = E_2' = \frac{\sqrt{s}}{2}. \tag{A.25}$$

The ratio β/β_1 is estimated by using equations (A.23) and (A.25):

$$\frac{\beta^2}{\beta_1^2} = \frac{E_\mathrm{B}^2 - m_p^2}{E_\mathrm{B} + m_\mathrm{P}} \cdot \frac{s}{s - 4m_\mathrm{P}^2}. \tag{A.26}$$

With $s = m_\mathrm{B}^2 + m_\mathrm{T}^2 + 2E_\mathrm{B}E_\mathrm{T} = 2m_\mathrm{P}^2 + 2m_\mathrm{P}E_\mathrm{B}$ follows:

$$\frac{\beta^2}{\beta_1^2} = \frac{(E_\mathrm{B} + m_\mathrm{P})(E_\mathrm{B} - m_\mathrm{P})}{E_\mathrm{B} + m_\mathrm{P}} \cdot \frac{2m_\mathrm{P}(E_\mathrm{B} + m_\mathrm{P})}{2m_\mathrm{P}(E_\mathrm{B} - m_\mathrm{P})} = 1. \tag{A.27}$$

The product of the tangents of the angles θ_1 and θ_2 yield with equations (A.19) and (A.27) to:

$$\begin{aligned} \tan(\theta_1) \cdot \tan(\theta_2) &= \frac{\sin(\theta_1')}{\gamma(\cos(\theta_1') + 1)} \cdot \frac{\sin(\theta_1')}{\gamma(-\cos(\theta_1') + 1)} \\ &= \frac{\sin^2(\theta_1')}{\gamma^2(1 - \cos^2(\theta_1'))} \\ &= \frac{1}{\gamma^2}. \end{aligned} \tag{A.28}$$

A.2 Wiring of the V1495 module

All input and output signals connected to the V1495 module are listed in the following tables.

Port A wiring.

Port	Mezzanine board	Nr	In/Out	configuration	Description
A	LVDS/ECL/PECL Input	0	In	RingL0	Signal of left semiring 1
		1	In	RingL1	Signal of left semiring 2
		2	In	RingL2	Signal of left semiring 3
		3	In	RingL3	Signal of left semiring 4
		4	In	RingL4	Signal of left semiring 5
		5	In	RingL5	Signal of left semiring 6
		6	In	RingL6	Signal of left semiring 7
		7	In	RingL7	Signal of left semiring 8
		8	In	RingL8	Signal of left semiring 9
		9	In	RingL9	Signal of left semiring 10
		10	In	RingL10	Signal of left semiring 11
		11	In	RingL11	Signal of left semiring 12
		12	In	RingL12	Signal of left semiring 13
		13	In	d-p left	trigger signal from edm config
		14	In	d-p right	trigger signal from edm config
		15	In		
		16	In	RingL13	Signal of left semiring 14
		17	In	RingL14	Signal of left semiring 15
		18	In	RingL15	Signal of left semiring 16
		19	In	RingL16	Signal of left semiring 17
		20	In	RingL17	Signal of left semiring 18
		21	In	RingL18	Signal of left semiring 19
		22	In	RingL19	Signal of left semiring 20
		23	In	RingL20	Signal of left semiring 21
		24	In	RingL21	Signal of left semiring 22
		25	In	RingL22	Signal of left semiring 23
		26	In	RingL23	Signal of left semiring 24
		27	In	RingL24	Signal of left semiring 25
		28	In	RingL25	Signal of left semiring 26
		29	In	RingL26	Signal of left semiring 27
		30	In	RingL27	Signal of left semiring 28
		31	In	RingL28	Signal of left semiring 29

Port B wiring.

Port	Mezzanine board	Nr	In/Out	configuration	Description
B	LVDS/ECL/PECL Input	0	In	RingR0	Signal of right semiring 1
		1	In	RingR1	Signal of right semiring 2
		2	In	RingR2	Signal of right semiring 3
		3	In	RingR3	Signal of right semiring 4
		4	In	RingR4	Signal of right semiring 5
		5	In	RingR5	Signal of right semiring 6
		6	In	RingR6	Signal of right semiring 7
		7	In	RingR7	Signal of right semiring 8
		8	In	RingR8	Signal of right semiring 9
		9	In	RingR9	Signal of right semiring 10
		10	In	RingR10	Signal of right semiring 11
		11	In	RingR11	Signal of right semiring 12
		12	In	RingR12	Signal of right semiring 13
		13	In	d-p up	trigger signal from edm config
		14	In	d-p down	trigger signal from edm config
		15			
		16	In	RingR13	Signal of right semiring 14
		17	In	RingR14	Signal of right semiring 15
		18	In	RingR15	Signal of right semiring 16
		19	In	RingR16	Signal of right semiring 17
		20	In	RingR17	Signal of right semiring 18
		21	In	RingR18	Signal of right semiring 19
		22	In	RingR19	Signal of right semiring 20
		23	In	RingR20	Signal of right semiring 21
		24	In	RingR21	Signal of right semiring 22
		25	In	RingR22	Signal of right semiring 23
		26	In	RingR23	Signal of right semiring 24
		27	In	RingR24	Signal of right semiring 25
		28	In	RingR25	Signal of right semiring 26
		29	In	RingR26	Signal of right semiring 27
		30	In	RingR27	Signal of right semiring 28
		31	In	RingR28	Signal of right semiring 29

Port C wiring.

Port	Mezzanine board	Nr	In/Out	configuration	Description
C	LVDS Output	0			
		1			
		2			
		3			
		4			
		5			
		6			
		7			
		8			
		9			
		10			
		11			
		12			
		13			
		14			
		15			
		16			
		17			
		18			
		19			
		20			
		21			
		22			
		23			
		24			
		25			
		26			
		27			
		28			
		29			
		30			
		31			

Port D wiring.

Port	Mezzanine board	Nr	In/Out	configuration	Description
D	A395A LVDS/ECL/PECL Input	0	In	energyBit0	Bit pattern to select mask: 000:direct, 001:mask1, 010:mask2, 011:mask3, 100:mask4
		1	In	energyBit1	
		2	In	energyBit2	
		3	In	SPinBits	Spin bits, direct linked to VME readout
		4	In		
		5	In		
		6	In		
		7	In	RF On/Off	linked to VME readout
		8	In	FlatTop	FlatTop bits linked to VME readout
		9	In		
		10	In		
		11	In		
		12	In		
		13	In		
		14	In		
		15	In		
		16	In	barF 01-04	signal from bars front
		17	In	barF 05-08	signal from bars front
		18	In	barF 09-12	signal from bars front
		19	In	barF 13-16	signal from bars front
		20	In	barF 17-20	signal from bars front
		21	In	barF 21-24	signal from bars front
		22	In	barF 25-28	signal from bars front
		23	In	barF 29-32	signal from bars front
		24	In	barB 01-04	signal from bars back
		25	In	barB 05-08	signal from bars back
		26	In	barB 09-12	signal from bars back
		27	In	barB 13-16	signal from bars back
		28	In	barB 17-20	signal from bars back
		29	In	barB 21-24	signal from bars back
		30	In	barB 25-28	signal from bars back
		31	In	barB 29-32	signal from bars back

Port E wiring.

Port	Mezzanine board	Nr	In/Out	configuration	Description
E	A395C ECL Output	0	Out	leftTrig	signal to timestamp
		1	Out	rightTrig	signal to timestamp
		2	Out	upTrig	signal to timestamp
		3	Out	downTrig	signal to timestamp
		4	Out		
		5	Out		
		6	Out		
		7	Out		
		8	Out		
		9	Out		
		10	Out		
		11	Out		
		12	Out		
		13	Out		
		14	Out		
		15	Out		
		16	Out		
		17	Out		
		18	Out		
		19	Out		
		20	Out		
		21	Out		
		22	Out		
		23	Out		
		24	Out		
		25	Out		
		26	Out		
		27	Out		
		28	Out		
		29	Out		
		30	Out		
		31	Out		

Port F wiring.

Port	Mezzanine board	Nr	In/Out	configuration	Description
F	A395C ECL Output	0	Out	Out	ScalerLeft13
		1	Out	Out	ScalerLeft14
		2	Out	Out	ScalerLeft15
		3	Out	Out	ScalerLeft16
		4	Out	Out	ScalerLeft17
		5	Out	Out	ScalerLeft18
		6	Out	Out	ScalerLeft19
		7	Out	Out	ScalerLeft20
		8	Out	Out	ScalerLeft21
		9	Out	Out	ScalerLeft22
		10	Out	Out	ScalerLeft23
		11	Out	Out	ScalerLeft24
		12	Out	Out	ScalerLeft25
		13	Out	Out	ScalerLeft26
		14	Out	Out	ScalerLeft27
		15	Out	Out	ScalerLeft28
		16	Out	Out	ScalerRight13
		17	Out	Out	ScalerRight14
		18	Out	Out	ScalerRight15
		19	Out	Out	ScalerRight16
		20	Out	Out	ScalerRight17
		21	Out	Out	ScalerRight18
		22	Out	Out	ScalerRight19
		23	Out	Out	ScalerRight20
		24	Out	Out	ScalerRight21
		25	Out	Out	ScalerRight22
		26	Out	Out	ScalerRight23
		27	Out	Out	ScalerRight24
		28	Out	Out	ScalerRight25
		29	Out	Out	ScalerRight26
		30	Out	Out	ScalerRight27
		31	Out	Out	ScalerRight28
G	NIM/TTL Selectable	0	In		
		1	In		

Statutory declaration

I declare that I have authored this thesis independently, that I have not used other than the declared sources and resources, and that I have explicitly marked all material which has been quoted.

Aachen, October 14, 2013

Fabian Hinder

Eidesstattliche Erklärung

Ich versichere, dass ich die Arbeit selbstständig verfasst und keine anderen als die angegebenen Quellen und Hilfsmittel benutzt sowie alle Zitate kenntlich gemacht habe.

Aachen, den 14. Oktober 2013

Fabian Hinder